∞

Dedicated to my wife, Nadya,

who encouraged me to aspire heights and ignore any limitations that got in the way,

since all limitations are simply waiting there for someone to break them.

∞

May 2014

Abstract

The main challenge of extracting the maximum power available from serially connected photovoltaic (PV) elements is the need for different bias operation currents. Generally, in order to overcome this challenge, DC-to-DC converters or micro inverters (DC-to-AC) are used to load every PV element by its maximum power point (MPP) load. Recently, an increased research effort has been invested in an alternative solution based on a differential power processing architecture. The main profit of this architecture lies in the processing of only the necessary differential power for all the PV elements MPP operation.

This study introduces an enhanced differential power processor topology for photovoltaic systems that is based on resonant-switched-capacitor technology, featuring local digital maximum power point tracking (MPPT) capability. The new converter operates as a voltage-dependent current source and is regulated by dead-time or frequency control. In addition, a normalized dynamic-gain MPPT algorithm for PV systems is presented while dealing with issues that originate from the digital control. The method demonstrates a rapid and uniform convergence toward the MPP by employing normalized dynamic steps while maintaining MPPT control compatibility that is suited for both differential and centralized power processors (e.g., DC-to-AC inverters). Theoretical analyses for the resolution effects on limit cycle oscillations and power curve traps in the MPPT process have been carried out and potential remedies have been applied and examined. The dynamic gain MPPT algorithm and the theoretical derivation have been verified on a 2 kW PV system using 150 W prototypes of bi-directional differential power processing setup. The experimental setup demonstrates a peak power-harvesting improvement of 42% and a general power-harvesting capability of above 90% and up to 99% out of the available power in the string, under different insolation levels.

Thesis Overview

The thesis deals with photo-voltaic power harvesting methodology. The work covers aspects of digital control together with a variety of hardware design issues based on switch-mode power supply systems. The digital control part of the work offers a wide comprehensive analysis for a suitable digital maximum power point algorithm and gives a wide analysis on the significant aspects of digital control. The other part of the work deals with aspects of the power harvesting system, concentrating on the mismatch problem solution. The core chapters of the work (2–5) content can be divided into three general independent subjects: Chapter 2 addresses the design and analysis of the DC to DC converter's hardware (i.e. power stage), Chapter 3 relates to the maximum power point tracking methodology, Chapter 4 deals with the digital control issues, and Chapter 5 concludes the comprehensive experimental work that includes the verification of the discussed issues. Earlier reports that summarize parts of this work were presented in a number of publications: Chapter 2 is based on [1] and [2], Chapters 3 and 4 are based on [3] and Chapter 5 concludes the experimental results of [1] and [3] using previous research results from [4] and [5].

Furthermore, the thesis constitutes the base fundamental methodology for ongoing research on a sub-module (PV cells) chain-connected DC to DC converters.

Acknowledgments

I would like to thank my supervisor Dr. Mor Mordechai Peretz, for encouraging me to trust my common sense while tackling state-of-the-art power electronics difficulties. Dr. Peretz inspired me with his enthusiasm in research creation. Dr. Peretz taught me how to analyse and solve any issue that appears in the way by finding the interesting magic in each and every problem.

I would like to thank my supervisor Prof. Shmuel (Sam) Ben-Yaakov, with whom I've worked for one intensive year. Prof. Ben-Yaakov taught me how to precisely phrase my written work and accomplish excellence without compromise.

I want to thank Mr. Alon Cervera for being a special friend that always offers his unconditional help and true, firm support. I have learned from Mr. Cervera more than I can tell. I wish him good luck in his PhD studies, his further academic career, and his personal life.

I would also like to thank my office colleagues from our research group and from others for all the constructive dialogues and for all the comic relief. I want to thank the administrative staff—Nili Grinberg and Azrikam Yehieli—for their support and help.

With great gratitude I thank my close and warm family. I want to thank my son, Ariel, for bringing so much joy and energy to my life. My wife, Nadya, for her great love and support, for her help putting things in their right proportions, and providing me with the time needed for my research work. I want to thank my parents and brother for their support and care.

Last but not least I would like to thank the funds that supported my research:

- THE ISRAEL SCIENCE FOUNDATION (grant No. 517/11)
- KAMIN – Ministry of Industry, Trade and Labor

without whom the research could not have been conducted.

Table of Contents

Figure List

Table List

Acronyms and Abbreviations

SMPS – Switch-mode power supply
SIC – Switched inductor converter
SCC – Switched capacitor converter
RSCC – Resonant switched capacitor converter
GRSCC – Gyrator resonant switched capacitor converter
MOSFET – Metal oxide semiconductor field effect transistor
CMOS – Complementary metal oxide semiconductor
IC – Integrated circuit
DCM – Discontinuous conduction mode
PDM – Pulse density modulation
MCU – Micro controller unit
ZCS – Zero current switching
PV – Photo voltaic
PVE – Photo voltaic element
GCI – Grid connected inverter
HC – Hill climbing
P&O – Perturb and observe
IncCond – Incremental conductance
LRCM – linear reoriented coordinates method
AMVL – adjustable matched virtual load
IVMPPE – *I–V* curves and maximum power point estimation
LCO – Limit cycle oscillations
ZEB – Zero error bin
PCT – Power curve traps
DPP – Differential power processor
SPP – Serial power processor
EQSCC – Equalizing switched capacitor converter

Inline References Legend

X.XX – Section / Chapter number
(X.XX) – Equation
[XX] – Reference
Fig. X.XX – Figure

1. Introduction

1.1. *Switch-mode power supply (SMPS)*

THE main subject of power electronics is energy processing by electronic circuits. An essential element of this field is the switch-mode power supply (SMPS) unit, which receives electrical power in one form at its input and produces electrical power in another form at its output, governed by the control system. The common components of the SMPS traditionally comprise a switched reactive element and input/output capacitive components. Another possible configuration is the switched-capacitor converter (SCC), which consists only of capacitive components, where at least one of them is a flying capacitor that flips between different states.

Switch-mode technology is essential to almost all systems that are powered by electricity, ranging from military systems (e.g. satellite, laser, and aircraft systems) to consumer electronics (e.g. computer, cellular, and general multimedia systems). High-frequency pulse width modulation (PWM) is the most popular principle of operation. This method controls the switch conduction period, and hence rules the input-to-output ratio. The reactive component implemented switch-mode power supplies with ideal switches are designed to have a theoretical power conversion efficiency of 100 %. Switch-mode technology is essential for applications of alternative energy sources in order to deliver regulated energy from a power source to a load with high efficiency while maintaining the source and load requirements, such as voltage level, output power, and response time.

1.2. *Photo-voltaic elements (PVE) - energy harvesting*

Harvesting the generated energy of a photo-voltaic system demands a SMPS unit to process the energy from its original form to the load designated form (i.e. from the PVE DC level to the grid ac level or to another DC battery storage level). In the general case of a grid-connected PVE system, the SMPS unit is usually referred to as a grid-connected inverter (GCI). Every PVE has its own output non-linear characteristics which are interpreted to a certain power

curve. The power curve characteristics of the PVE are mainly dependent on the element's temperature, its degradation level, and the irradiance condition [6]. Loading the PVE by its suitable maximum power point (MPP) load is necessary to harvest all of the latent power available in the element. Since the MPP load is determined according to its specific present power curve i.e. its surrounding conditions, it is being changed most often. Tracing the needed MPP load value is usually performed by a maximum power point tracing (MPPT) circuitry or algorithm. Estimating the necessary load from its surrounding conditions is not practical, so in most cases the MPPT control circuitry samples the output of the panel and varies its load until the maximum power is obtained. Since the panel is loaded by the GCI, the MPPT system is usually utilized as a part of a GCI control algorithm. Thus, the input impedance of the GCI is frequently adjusted to provide the optimum load for the PVE.

1.3. *MPPT algorithms*

Tracking the MPP of the PVE is of major concern in many solar-energy harvesting systems (not only at GCIs). Recently, the realization of MPPT that is compatible for various mismatch conditions of the PVE systems has received increased attention [7], [8]. Environmental conditions such as shading (full or partial), non-homogeneous dirt and defects result accelerate degradation of the PVE [9] and, as a consequence, alter the characteristics of the PVE, introducing two or more local power peaks rather than one global MPP. A wide variety of works propose MPPT algorithms with main objectives: to track the MPP as fast and as accurate as possible, yet implementing a simple hardware harvesting system.

1.3.1. *Hill Climbing (HC), and Perturb and Observe (P&O)*

Among all the works gathered in this thesis scope dealing with MPPT algorithms, much focus has been on hill climbing (HC) [10]–[16] and perturb and observe (P&O) [17]–[28] methods. Hill climbing involves a change in the correction signal of the power converter, sensing the power trend due to that change, and forcing another change on the correction signal until the sensed trend is in the vicinity of zero. On the other hand, the P&O perturbs back and forth the operating voltage of the PV array and corrects the referred target voltage as the HC fixes its correction signal. In the case of a PV array connected to a power converter, perturbing the duty ratio of the power converter perturbs the PV array current and consequently perturbs the PV array voltage. Hill climbing and P&O methods are different ways to envision the same fundamental method.

The advantage of the HC and P&O MPPT methods is their simplicity. However, it was proved that a P&O MPPT control system sometimes deviates from the maximum operating point in the case of rapidly changing atmospheric conditions, such as broken clouds [29]. This problem could happen with the adaptive hill climbing method as well. When a sudden increase or decrease in insolation dominates the change of PV output power, according to the HC tracking algorithm, the controller may be confused and lead the operating point in the wrong direction. This process continues until the sudden change in insolation slows down or stops. Another disadvantage [30] is that this simple tracking method has difficulty in providing good performance in both dynamic and steady-state response because a constant incremental step of duty cycle was adopted as the control parameter. If the incremental step of the duty cycle is small, the backing time is long and the system shows poor dynamic response. If a large duty cycle step is used, the output power fluctuations are large and the average power is significantly less than the maximum, resulting in energy waste (Fig. 1.1). Therefore, works that modify the HC MPPT algorithm employ an adaptive tracking step size [31] to facilitate the MPP convergence time without suffering large output fluctuations around the MPP.

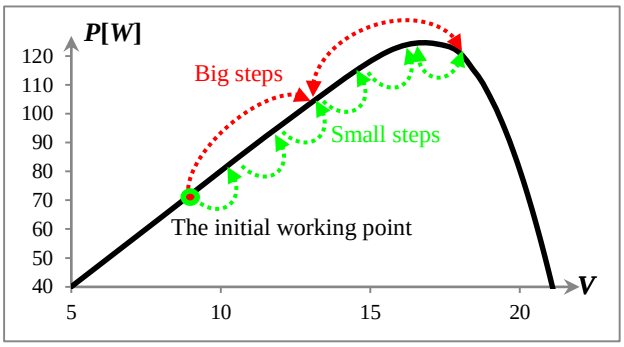

Fig. 1.1 Illustration of convergence to MPP by HC MPPT with small (green) and big (red) steps.

1.3.2. *Incremental conductance (IncCond)*

The IncCond (IncCond) method [17], [29], [32]–[41], [43] is based on the PV array power curve slope (Fig. 1.1). The slope at the MPP vicinity is approximately zero, positive at lower voltage, and negative at higher voltage, as given by

$$\begin{cases} \mathrm{d}P/\mathrm{d}V \approx 0, & V \approx V_{\mathrm{MPP}} \\ \mathrm{d}P/\mathrm{d}V > 0, & V < V_{\mathrm{MPP}} \\ \mathrm{d}P/\mathrm{d}V < 0, & V > V_{\mathrm{MPP}} \end{cases}, \tag{1.1}$$

where V_{MPP} is the PVE MPP voltage. The power can be expressed as the product of the voltage and the current so that the derivative of the power can be expressed as:

$$dP/dV = d(V \times I)/dV = I + V \times (dI/dV), \tag{1.2}$$

and if we indicate ΔI and ΔV as the subtraction of the last MPP iteration sensed signal from the present sensed signal (current and voltage, respectively), assuming small step size in ΔI and ΔV,

$$dP/dV \approx I + V \times (\Delta I/\Delta V). \tag{1.3}$$

Using (1.1), the expression (1.3) can be rewritten as

$$\begin{cases} \Delta I/\Delta V \approx -I/V, & V \approx V_{MPP} \\ \Delta I/\Delta V > -I/V, & V < V_{MPP} \\ \Delta I/\Delta V < -I/V, & V > V_{MPP} \end{cases}. \tag{1.4}$$

The MPP can thus be tracked by comparing the instantaneous conductance (I/V) to the incremental conductance ($\Delta I/\Delta V$). It is common to refer IncCond as a subset of the HC MPPT family since it involves a change in the correction signal of the power converter and not necessarily perturbs back and forth the operating voltage. Therefore IncCond has the same trade-off between a small or a big step size in the correction signal as the HC method. However, the methods proposed in [36] and [44] use a different MPPT algorithm to bring the operating point of the PVE close to the MPP in the first stage and in the second stage use IncCond to track the accurate MPP. This two-stage alternative also ensures that the real MPP is tracked in case of multiple local maxima. The work done in [45] combines a method of a linear function and the IncCond. The linear function is used to divide the *I*–*V* plane into two areas and contains all the possible MPPs under changing atmospheric conditions. The presented method resembles [46] in that it presents the adjustable matched virtual load (AMVL) method. The operating point is brought into the MPP area by the AMVL MPPT method and then IncCond is used to reach the accurate MPP. The AMVL method is biased on a line that contains all the possible MPPs under changing atmospheric conditions and meanwhile fine-tunes it according to the changing of the environmental condition changings by P&O or IncCond.

Another effective way of performing the IncCond technique is to use the instantaneous conductance and the IncCond to generate an error signal

$$e = \frac{\mathrm{d}P}{\mathrm{d}V} = \frac{I}{V} + \frac{\mathrm{d}I}{\mathrm{d}V} \tag{1.5}$$

as suggested in [33] and [34]. From (1.1), we know that *e* goes to zero at the MPP. A simple proportional integral (PI) control can then be used to drive *e* to zero. Measurements of the instantaneous PVE voltage and current require two sensors. The IncCond method lends itself well to microcontrollers and DSP control, which can easily sense the voltage and current, and keep track of their previous values and make all the decisions as described earlier.

1.3.3. *Maximum power point estimation*

The general objective of the MPP estimation is to propose an alternative MPPT algorithm that can trace the MPP by estimating its voltage, current, or load characteristics from previous sensed data. This MPPT family obtains MPP with much less signal sensing (PVE's voltage/current) and in most cases does it faster. Its drawback is concealed in its large possible diversion error. The method discussed in [47] predicts the MPP by manipulating the PVE characteristic equation iteratively. In this way, it is solved and an approximate symbolic solution for the MPP is found. This method, called the linear reoriented coordinates method (LRCM), requires the measurement of V_{OC} and I_{SC} to find the solution. Other constants representing the PVE characteristic curve are also needed. The maximum error in using LRCM to approximate the MPP was found to be 0.3%, but this was based only on simulation results and clearly inherent additional power losses are present in the V_{OC} and I_{SC} sampling operation. Another work based on a similar technique [48] presents a practical implementation of a photovoltaic *I*–*V* curves and maximum power point estimation algorithm (IVMPPE). The IVMPPE estimates the *I*–*V* curve by measuring six voltage and current coordinates near the operating point and sets the operation of the solar panels at its MPP voltage without tracking.

In [48], a sliding mode control method with a buck-boost converter is used to achieve MPPT. This method defines the switching function *u* of the converter and determines it by using (1.1) (mentioned in the IncCond algorithm) such that *u* is expressed as

$$\begin{cases} u = 0, & S \geq 0 \\ u = 1, & S < 0 \end{cases}, \tag{1.6}$$

where $u = 0$ means the switch is open and $u = 1$ means the switch is closed and the sliding surface, *S*, is given by

$$S = \frac{\mathrm{d}P}{\mathrm{d}V} = I + V\frac{\mathrm{d}I}{\mathrm{d}V}. \tag{1.7}$$

A similar method combined with the AMVL method [50] is further developed in [51] using a boost converter.

1.4. *Effects of Digital control*

Most modern MPPT algorithms are realized using digital processing control systems. As a result, issues related to digital control such as sampling resolutions of both current and voltage may introduce undesirable behavior. Power curve traps (PCT) [52] and/or limit cycle oscillations (LCO) [53]–[55] may be of major concern for successful MPPT implementation.

1.4.1. *Limit cycle oscillations (LCO)*

In digitally controlled SMPS with a single voltage feedback loop, the two quantizers, namely the analog-to-digital converter (ADC) unit and the digital pulse-width modulator (DPWM), can cause undesirable limit-cycle oscillations (LCO). Analytical analysis reveals that DPWM-controlled SMPS, limit cycles occur when the LSB of the control (described as v_q in Fig. 1.2) changes the output (described as v_o in Fig. 1.2) by a value that is larger than ADC resolution.

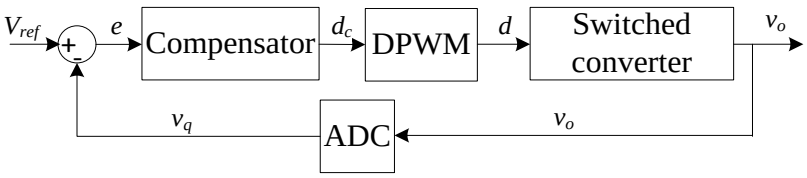

Fig. 1.2 Controlled SMPS - Block diagram

Generally, based on that logic, the existence condition of LCO can be determined as:

$$\Delta v_{o\min} > q_{ADC}, \tag{1.8}$$

where $\Delta v_{o\min}$ is the minimal output voltage change, i.e. the change for a LSB duty ratio in the DPWM unit, and q_{ADC} is the ADC quantization (resolution) value. So by expressing $\Delta v_{o\min}$ as:

$$\Delta v_{o\min} = G_O \times Q_{DPWM}\left(d_c\right) \times G_{CO} \times K_{ADC}, \tag{1.9}$$

where G_O is the DC control-to-output gain of the converter, Q_{DPWM} is the DPWM quantization (resolution) value, G_{CO} is the DC gain of the compensator, and K_{ADC} is the output voltage sensing gain. From (1.8) and (1.9) the existence condition of LCO can be finally determined as:

$$G_O \times Q_{DPWM}\left(d_c\right) \times G_{CO} \times K_{ADC} > q_{ADC} \tag{1.10}$$

1.4.2. *Power traps* [52]

Power traps appear as local maxima in the measured power curve of a PVE (Fig. 1.3, Fig. 1.4). Those power traps are caused by electromagnetic interference of the SMPS harvest unit switching transients (commonly called "noise") and other deterministic phenomena (e.g. ADC quantization error) in the sensed PVE unit. Traps exist even in the absence of shading and degrade the performance of all MPPT methods.

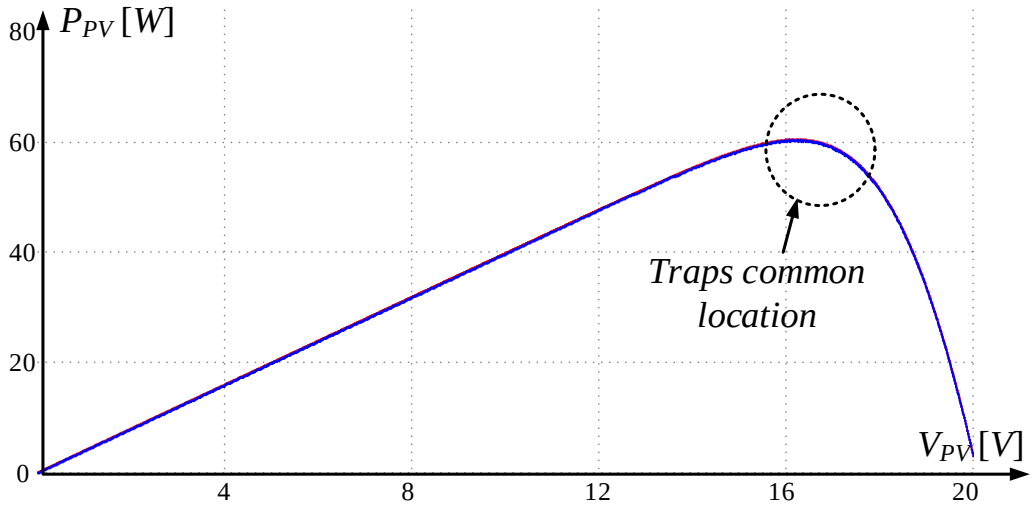

Fig. 1.3 Power versus voltage for simulated two PV panels (quantized sensed power in blue and continuous power in red) at 1000 W/m^2, with and without a measurement trap.

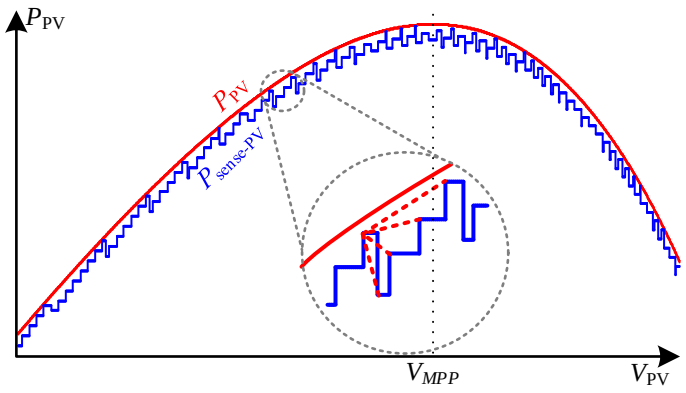

Fig. 1.4 Close-up of Fig. 1.3 at trap location.

1.5. *Mismatch effect on serially connected PVEs*

Different insolation levels, degradation, and temperature differences tend to impact the PVE MPP characteristics. But the most common of those issues is the different insolation problem that mainly impacts the MPP current [6]. Therefore, full or partial shading of PVEs, which are part of a serially connected array, limits the power that can be extract from the chain [24], [56], [57]. The serial connection forces the same current through the mismatched PVEs (Fig. 1.5) causing one (or more) of the PVEs to digress from its MPP.

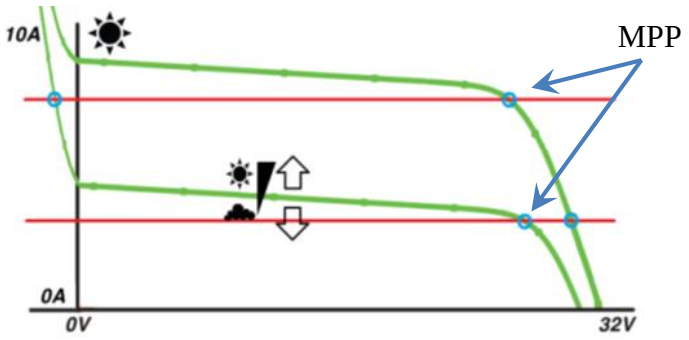

Fig. 1.5 PV panel current–voltage curves in different insolation levels.

For simplification, observing the power–voltage curve of two serially connected PVEs in Fig. 1.6 clearly reveals two local MPPs that reach much lower MPP from the absolute potential MPP of the two connected panels. The absolute potential MPP is defined by separate harvesting conditions with no connection of the two PVEs. It is noteworthy that the power differences depend on the mismatch levels (Fig. 1.7).

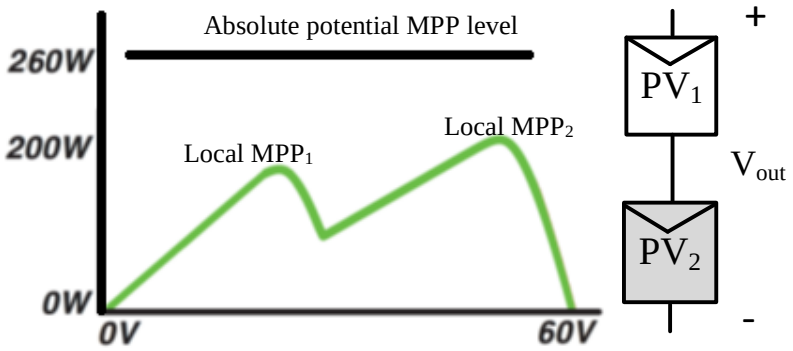

Fig. 1.6 Two PV panel output power-to-voltage curves in different insolation levels.

To illustrate the non-harvested power due to shading differences, Fig. 1.7 demonstrates the difference between the higher local MPP of two serially connected panels and their absolute available maximum power. Fig. 1.7 relates to the harvested power ratio as ξ:

$$\xi = P_{out} / \left(P_{\mathrm{PV1}} + P_{\mathrm{PV2}} \right) \times 100\%, \tag{1.11}$$

where $P_{\mathrm{PV}i}$ is the i^{th} PV panels maximum power and P_{out} is the higher local MPP.

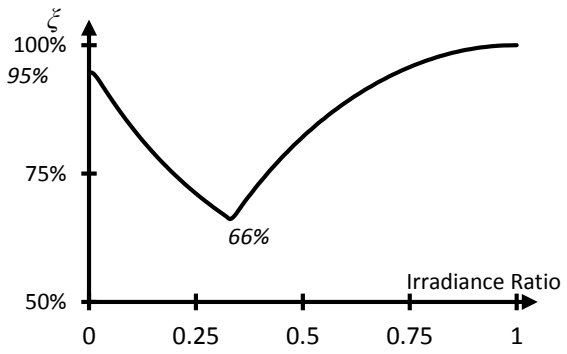

Fig. 1.7 Harvested power percentage from the total available power for different irradiance (two connected PV panels).

1.6. *Literature survey – PVE's dedicated converters and architectures*

A variety of proposed literature and industrial solutions attempt to obtain the maximum power available in serially connected PVE chains. Generally, two groups of power processing solutions have been proposed to remedy the shading problem. One group is based on a dedicated converter/inverter per element [58]–[60]. The other group of solutions keeps the series connection of the elements intact and processes mismatched currents due to the shaded unit(s) using parallel circuitry [61]–[64]. The work of [65] and [66] present a comparison between these methods. The latter has the advantage of processing only the power differences between the PV elements, thus minimizing conversion losses and improving reliability.

1.6.1. *Serially Power Processing (SPP)*

Serially connected power converters (per panel) provide an alternative topology to a simplified dc–ac inverter that creates a high voltage PVE string providing the MPP of each connected PVE. This offers the advantages of a "converter-per-panel" approach without the cost or efficiency penalties of individual dc–ac grid connected micro inverters. The work presented at [59] provides a system implementation based on a buck-boost topology,

where [67] compares the different implementation topologies for this architecture (boost, buck, buck-boost, and Ćuk converters). A wider comparison of this architecture is given in [68].

1.6.2. *Differential power processing (DPP)*

A unique advantage of the differential power processing architecture is that MPPT can be obtained locally, in each PVE, by processing only the necessary amount of power needed to achieve MPP. Several converter realizations have been proposed as candidates for differential power processors (DPP), mainly derived from battery management applications [69], [70]. An equalizing switched capacitor converter (EQSCC) is proposed in [5] and [71] as a voltage equalizer with simple open-loop control, relying on the assumption that MPP voltage deviation due to change in irradiance level is negligibly small. This approach stands out in its simplicity, high self-efficiency, and lower cost. However, it lacks MPPT capability without introducing losses. A buck-boost topology has also been proposed, acting as an equalizer [63], and further developed in [64] to obtain local MPPT by differential processing to keep all PV units in MPP. However, compared to SCC technology of the same power level, it is bulkier in volume because of the large magnetic element required [72]. Furthermore, the MPP voltage of a PVE variation as a function of the irradiance is affected by the element's internal resistance and temperature. The resultant voltage drift may be either negative or positive with respect to the nominal MPP [6], [73], which highlights the need for a DPP with true tracking capabilities, i.e. step-up/down functionality. The concept of full local MPPT DPP has been initially introduced in [67], [74] and further developed and demonstrated in [64]. An overview of the possible architectures is presented in [66] and a comparison between their performances is given in [8]. To overcome the same PV mismatch problem in the sub module of the PV panel, a sub-module implementation for the DPP has been proposed in [75], [76].

1.7. *Gyrator resonant switched capacitor converter (GRSCC) [86]*

1.7.1. *Introduction*

The efficiency of most common SCCs is limited by their operating voltage ratio [77]–[81]. In such converters, the efficiency depends on the ratio of the output voltage to target voltage, V_O and V_T, respectively (i.e. V_T is the no load SCC output voltage); therefore, general SCC's efficiency can be expressed as $\eta = V_O/V_T$. Regulation can be obtained either by varying the SCC's components parameters, switching duty-cycle/frequency, or inserting a post regulation stage [82]–[84] to match the required conversion ratio. A more complicated approach for

voltage regulation by SCC is to generate multiple conversion ratios and therefore increase the effective operation range [80], [82]–[85]; the system efficiency, however, would remain of a discrete nature.

Resonant switched capacitor converter (RSCC) operation with zero current switching (ZCS) has been investigated with the aim to reduce the switching losses, allowing higher switching frequency operation. There, higher efficiency is obtained, yet limited by its conversion ratio and a discrete nature.

The gyrator resonant switched capacitor converter (GRSCC) topology in its generic form, as described in Fig. 1.8, requires bi-directional switches (Q_1, Q_2, and Q_3) that operate synchronously. This is required to support bi-directional and non-inverting step-up and -down capability in a single configuration. However, for more specific cases, such as unidirectional power flow and/or specific conversion types (up or down), the number of switches and the configuration complexity can be significantly reduced.

1.7.2. *Principle of operation*

The operation of the converter shown in Fig. 1.8 is described for a steady-state of charge/discharge/balance cycle and a dead-time state which turns all the switches (Q_1–Q_3) off to achieve current regulation. Fig. 1.9 illustrates the capacity voltage, V_C, and the resonant tank current, I_C, for the case of a non-unity step-up conversion. By turning Q_1 on, a charge state (S1) is started, which resonantly charges the flying capacitor from the input V_1. At zero current, Q_1 is turned off and after a while (dead-time) Q_2 is turned on (state S2). At this point, the flying capacitor resonantly discharges onto the output capacitor. Since the input voltage, V_1, and the output voltage, V_2, are of different values, only a portion of the charge is delivered to the output and results in V_C that is different from its voltage at the starting point of S1. V_C at this point (neglecting parasitics) is the negative value of its voltage at the beginning of S1. By turning Q_3 on (S3), the resonant tank is short-circuited. This creates the required charge-balance and reverses the flying capacitor voltage polarity such that the voltage at the end of S3 equals the voltage at the beginning of S1. Further description of the GRSCC operation can be found in [86].

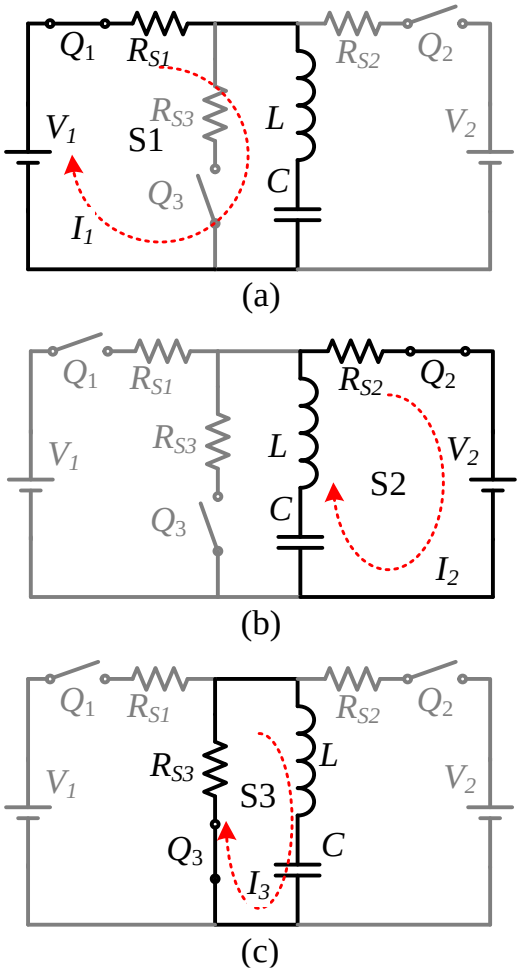

Fig. 1.8 GRSCC configuration and operation principle: (a) *charge*, (b) *discharge*, and (c) *balance* states [86].

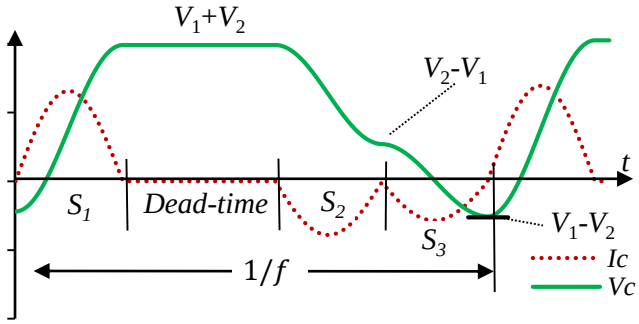

Fig. 1.9 Typical GRSCC waveforms of the flying capacitor voltage and current. The circuit parameters are: $V_1 = 20\,\mathrm{V}$, $V_2 = 31\,\mathrm{V}$, $R_S = 0.15\,\Omega$, $L = 5.2\,\mu\mathrm{H}$, $C = 0.25\,\mu\mathrm{F}$.

The maximal operating GRSCC frequency is ruled by the 2/3 of the resonant tank natural frequency, thus determined by:

$$f_{\max} = \frac{1}{3\pi\sqrt{LC}}, \tag{1.12}$$

and the general operating frequency is expressed as:

$$f = G \times f_{\max} = \frac{G}{3\pi\sqrt{LC}} \tag{1.13}$$

where $G \in (0,1]$ is defined as the regulation factor. In this mode of operation, the converter's output current will be determined by the input voltage and operating frequency as follows:

$$I_2 = 2f \times C \times V_1 \;;\; V_2 = \frac{1}{2f \times C} I_1 \tag{1.14}$$

The relationship between the maximum output current, I_2, passed from V_1 onto the output voltage, V_2, is a function of the capacitive and inductive components of the resonant tank (L, C), and can be expressed as:

$$I_2 = \frac{2}{3\pi \times Z} V_1 \;;\; Z = \sqrt{L/C} \tag{1.15}$$

The relationship between input voltage to output current of (1.14) with the relation of output voltage to input current is known as a gyrator. Hence, this topology realizes a frequency-regulated voltage-dependent current source; this topology is termed a gyrator resonant switched capacitor converter (GRSCC) [86].

2. Analysis and design of GRSCC as a DPP for serially connected PV elements

2.1. *Introduction*

Full or partial shading of a serially connected PV string severely impacts the power that can be extracted from it [56], [57]. Generally, two groups of power processing solutions have been proposed to remedy the shading problem. One group is based on a dedicated converter/inverter per element [58]–[60], whereas the other group of solutions keeps the series connection of the elements intact and processes mismatched currents due to the shaded unit(s) using parallel circuitry [61]–[64]. The latter is named differential power processing (DPP) architecture and has the advantage of processing only the power differences between the PV elements, thus minimizing conversion losses and improving reliability. Implementing this architecture by gyrator resonant switched-capacitor converter (GRSCC) units is the main subject of this chapter.

The superior capability of the DPP architecture over other possible systems lays on its local maximum power point tracking (MPPT) capability, in the PV element (PVE) level, by processing only the necessary amount of power needed to achieve maximum power point (MPP). Several converter realizations have been suggested as candidates of DPP. An equalizing switched capacitor converter (EQSCC), proposed in [5] and [71] as a voltage equalizer with simple open-loop control, relies on the assumption that MPP voltage deviation due to change in irradiance level is negligibly small. This approach stands out in its simplicity, high self-efficiency, and lower cost. However, it lacks MPPT capability without introducing losses or passing differential power from the low-voltage PVE onto its adjacent high-voltage PVE through the chain. Furthermore, the variation of the MPP voltage of a PVE is affected by the element's internal resistance and temperature. The resultant voltage drift may be either negative or positive with respect to the nominal MPP [6], [73], which highlights the need for a DPP with true tracking capabilities, i.e. step-up/down functionality.

This chapter introduces an enhanced DPP topology that incorporates the virtues of both switched-capacitor and switched-inductor converters in a newly developed current-sourcing converter that is based on resonant SCC technology (Fig. 2.1). The new converter is of low-volume, features high-efficiency with extended operation range, and is capable of performing

local MPPT. The chapter presents the new converter DPP topology, its principle of operation, and its components main design considerations.

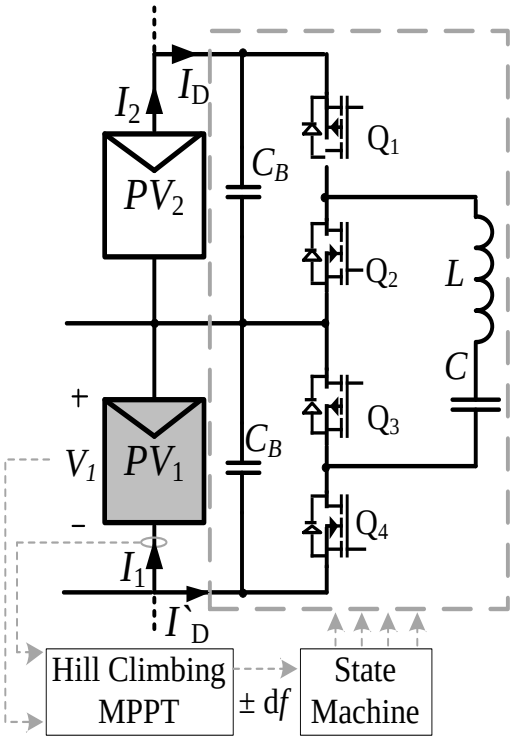

Fig. 2.1 DPP Conceptual hardware setup.

2.2. *Power flow*

The main goal of differential power processing in PV systems is to maximize the power conversion efficiency by processing only a small portion of the power being produced. The concept has been initially introduced in [74], [67] and further developed and demonstrated in [69]. The architecture is conceptually shown in Fig. 2.2. It consists of N serially connected PV elements and N–1 current sourcing converters connected in parallel with two adjacent PV elements. The differential power passes along the string in a so-called bucket-brigade pattern. Each converter performs local MPPT to one of its two connected PVEs by sinking or sourcing current to/from the neighboring PV element. A central grid-connected inverter is still used to interact with the grid and to track the global MPP. Effectively, it also performs the local MPPT for the N^{th} element.

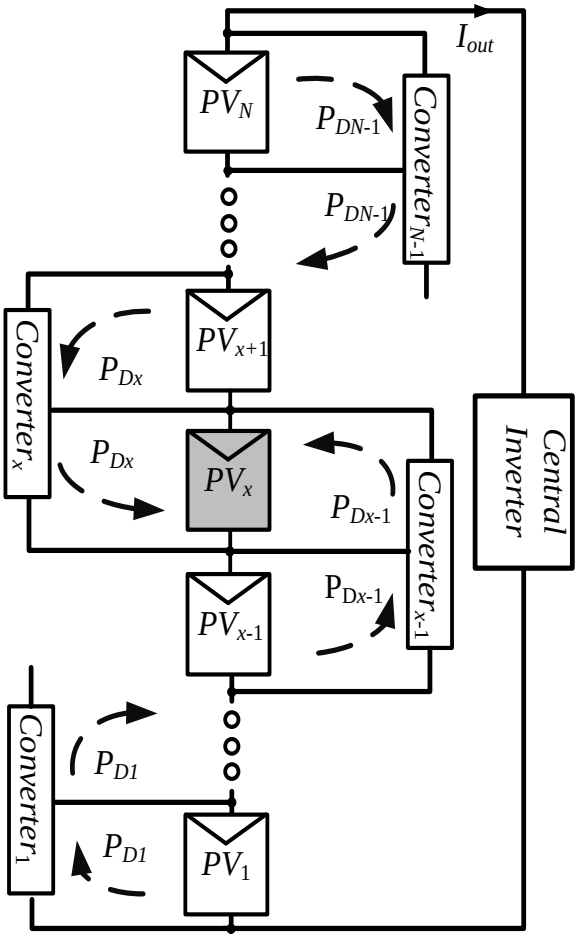

Fig. 2.2 Example of the power flow for a *N* PV panel string connected to *N*–1 gyrator DPPs, containing a shaded PV at the *x* location**.**

The differential converters are needed only in the case of mismatch in the MPPs, i.e. only a portion of the power is processed. The MPP is maintained for each of the PV elements owing to the differential current provided by the DPP. For example, the amount of power processed by each converter in a string of *N* elements in order to bring a single mismatched element (*PVx*, Fig. 2.2) to its MPP can be expressed as [5]:

$$P_{Dj} = \begin{cases} \dfrac{P_0 - P_S}{N} j & ; \quad j < x \\ \dfrac{P_0 - P_S}{N}(N - j) & ; \quad j \geq x \end{cases}, \tag{2.1}$$

where the index *j* represents the location of a converter in the string, P_s is the maximum power of the shaded element, and P_0 is the power of a non-shaded element at its MPP. For better illustration, consider an example of a string with five PV elements and the 3rd element is shaded,

then the power processed by the 3rd converter would be $(P_o\text{-}P_s)\times 2/5$. Further details on the distribution of the processed power can be found in [5].

It can be observed from (2.1) that converters adjacent to the shaded element are required to process most of the differential power whereas others located farther in the string contribute a smaller portion of the power, linearly proportional to their location with respect to the mismatched PV element. A current-sourcing converter that operates as a DPP is thus required to be bi-directional and capable of step-up and step-down operation. In addition, the power-flow behavior of this example indicates that some processed power needs to pass through a few converters until it reaches its destination (even though there is only one mismatched module within the string). This power-flow behavior explains the results of power processing probability comparing PV-to-PV and PV-to-bus architecture in [64]. It is important to take into consideration the expansion of processing losses of high-ratio voltage conversion and the system complexity at the PV-to-bus (isolated and non-isolated) architecture.

In the context of this study, the harvesting factor, ξ, is defined as the relationship between the total extracted power out of a serially connected string, P_{out}, and the sum of the absolute maximum power that can be harvested from each individual element, $P_{i,MPP}$, that is:

$$\xi = \frac{P_{out}}{\sum_{i=1}^{N} P_{i,MPP}} \quad . \tag{2.2}$$

Considering (2.1) and (2.2), it would be highly advantageous that the efficiency of the converter be independent of the operating conditions. Converter topologies such as switched-capacitor [70] or buck-boost [64], originally proposed for battery equalization and realized for PV applications, have many merits; however, their efficiency range is limited. SCC lacks MPPT capability [5]. In a buck-boost configuration, the efficiency range is somewhat limited around the nominal power level, and there is a trade-off between the size and performance of the converter.

To overcome these challenges, this study introduces a new DPP topology employing GRSCC. It combines the benefits of reduced size SCC and current sourcing properties with high efficiency over a wide range [86].

2.3. *Principle of operation*

The GRSCC configuration as a DPP is described in Fig. 2.1 similar to the architecture of a conventional EQSCC [5], [78]–[81], the DPP includes four switches and a resonant tank. Two PV elements connect as input and output sources.

As opposed to the operation of a classical SCC that includes a charge state and a discharge state, here an additional switching phase is introduced that breaks the rigid connection of the input/output voltage gain and the efficiency of the converter. Controlling the sequence of the switches governs the power-flow direction, hence bi-directional step up/down operation.

The operation of the GRSCC, shown in Fig. 2.3, is described for one steady-state charge/discharge/balance cycle and is assisted by the behavior shown in Fig. 2.4 that illustrates the capacitor voltage, V_C, and the resonant tank current, I_C, for a case of a MPP mismatch that requires a non-unity step-up conversion. By turning Q_1 and Q_3 on, a charge state (S1 — Fig. 2.3a) is commenced, which resonantly charges the flying capacitor from PV_2. At zero current, Q_1 and Q_3 are turned off and Q_2 and Q_4 are turned on (state S2 — Fig. 2.3b). At this point, the flying capacitor resonantly discharges onto PV_1. If PV_1 voltage, V_{PV1}, and PV_2 voltage, V_{PV2}, are of different values, only a portion of the charge is delivered to the output and results in V_C that is different than its voltage at the starting point of S1. The amount of this voltage difference (neglecting R_s — parasitic resistances in each loop) equals twice the residual voltage of the flying capacitor. By turning Q_2 and Q_3 on (S3 — Fig. 2.3c) the resonant tank is short-circuited. This creates the required charge balance and reverses the flying capacitor voltage polarity such that the voltage at the end of S3 equals to the voltage at the beginning of S1.

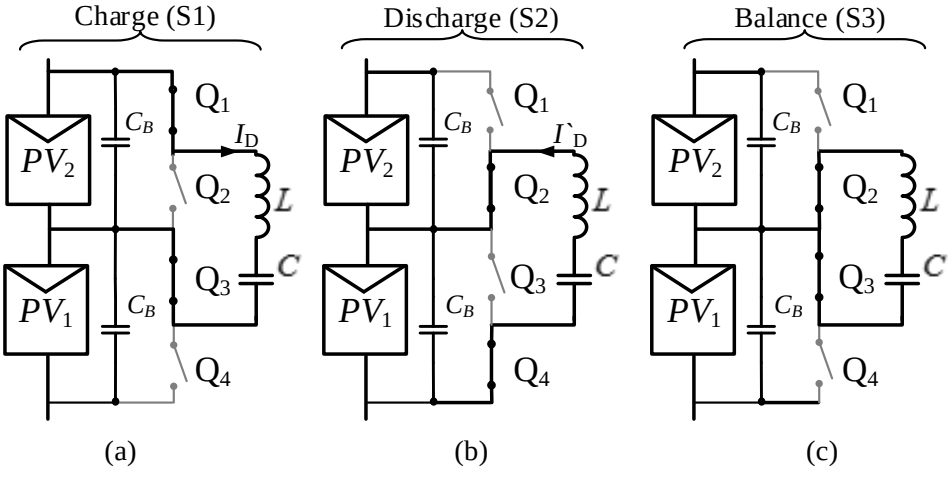

Fig. 2.3 The three states of the DPP GRSCC.

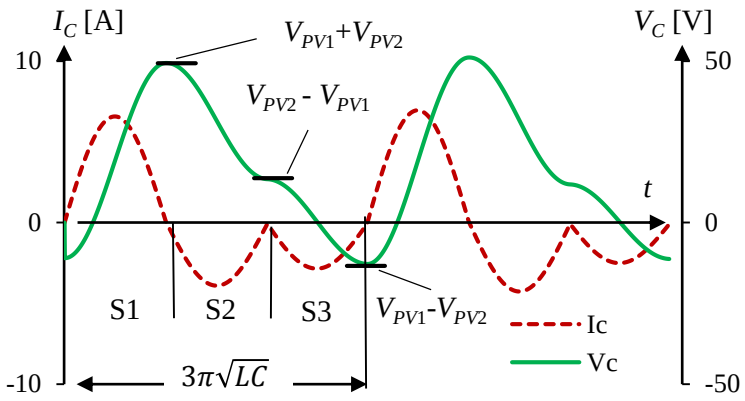

Fig. 2.4 Typical waveforms (obtained from simulation) of the flying capacitor voltage and current. Circuit parameters are: $V_{PV1} = 20\,\text{V}$, $V_{PV2} = 31\,\text{V}$, $R_s = 0.15\,\Omega$, $L = 5.2\,\mu\text{H}$, $C = 0.25\,\mu\text{F}$.

The addition of a third, charge-balancing state, to the switching sequence transforms the resonant SCC into a voltage dependent current-sourcing converter that, neglecting losses, is capable of accommodating any input to output voltage gain (larger and smaller than unity). It should be noted that the order of the switching sequence will govern the power flow direction.

To facilitate regulation of the amount of charge that is transferred to the output, a pulse density modulation (PDM) is employed [72], i.e. a time delay is introduced between the charge and the discharge states. The average currents (I_D, $I`_D$) (Fig. 2.1) and voltages (V_{PV1}, V_{PV2}) of the converter can be defined as a gyrator relationship [86]:

$$I_D = 2\,fC\,V_{PV2} \quad ; \quad V_{PV1} = \frac{1}{2\,fC} I`_D \ , \tag{2.3}$$

where f is the frequency of a cycle that includes the three states and the time delay. Maximum differential current is passed when no additional time delay is added. It can be observed from (2.3) that the differential current is inversely proportional to the time delay, but linearly proportional with f. This implies that controlling the differential current by the frequency as the correction signal is preferred, since variations in the time delay would result in a nonlinear behavior. Furthermore, the time resolution of a variable-frequency signal, generated by a local oscillator, is not constant and strongly depends on the operating point [87] which introduces additional nonlinearity. By modifying the correction signal to frequency, incremented by fixed

steps, d*f*, these nonlinearities are eliminated and the power converter can be treated as a constant gain block from frequency to current as prescribed in (2.3).

2.4. *Bridge design and analysis*

The relationship between the maximum current, I_{Dmax}, passed from PV_1 and the voltage on an adjacent element, PV_2, is a function of the capacitive and inductive components of the resonant tank (L, C), and can be expressed as:

$$I_{Dmax} = \frac{2}{3\pi Z} V_{PV2} \quad ; \quad Z = \sqrt{L/C} \ . \tag{2.4}$$

Assuming that identical parasitic resistances R_s exist in all three sub-circuits (Fig. 2.3), the expected efficiency of the converter can be estimated by:

$$\eta = \left[1 + \frac{\pi R_s}{2Z} \left(A + A^{-1} - 1 \right) \right]^{-1} \quad ; \quad A = \frac{V_{PV2}}{V_{PV1}} \ . \tag{2.5}$$

2.4.1. *Power stage - components design*

The values of the bridge inductor L and capacitor C are derived by combining (2.3) with (2.5), taking into account the extreme case of f_{max}, $V_{PV1,min}$ and $I_{D,max}$ as follows:

$$\begin{aligned} C &= \frac{I_{D,max}}{2 V_{PV,min} f_{max}} \\ L &= \left[\left(3\pi f_{max} \right)^2 C \right]^{-1} \end{aligned} \ , \tag{2.6}$$

where I_{Dmax} and f_{max} are a given maximum differential current and its maximum allowed operation frequency and $V_{PV,min}$ is the minimal MPP voltage of the PVE for which the GRSCC is designed to work.

The components generalizing the charge/discharge parasitic resistance R_s limits the converter's efficiency (2.5). R_s includes the MOSFETs' 'on' resistance, R_{DSon} value and the equivalent series resistance of the capacitor/inductor, ESR_C/ESR_L. Using (2.5) with the maximal voltage expected ratio and a given efficiency, the designed parasitic resistance can be expressed by:

$$R_S = R_{DSon} + ESR_C + ESR_L = \frac{2Z \times \left(\eta^{-1} - 1 \right)}{\pi \left(A_{\max} + A^{-1}{}_{\max} - 1 \right)} . \tag{2.7}$$

The gate drive system uses a simple DC restorer method implemented by passive components and widely discussed in [4]. This method is employed because of its simplicity and stable DC referred source compatibility of the driven MOSFET terminal.

The output voltage ripple of the converter primarily depends on the ratio between the resonant tank capacitance, C, and the bus capacitance, C_B (in parallel to the PV element), as detailed in [72], [86]. Therefore, using the relation of the capacitance, the PVE voltage, and its voltage ripple provided in [72], [86], the capacitance value of C_B can be expressed by:

$$C_B = C\frac{2V_{PV,min}}{\Delta V_{2,p-p}} \tag{2.8}$$

where $\Delta V_{2,p\text{-}p}$ is the system tolerable PVE voltage ripple.

3. MPPT algorithm

3.1. *Introduction*

Tracking the MPP of photovoltaic elements is of major concern in many solar energy harvesting systems. Recently, the realization of MPPT that is compatible for various mismatch conditions of the PV array has received increased attention [7]. Environmental conditions such as shading (full or partial), non-homogeneous dirt, and defects result in accelerated degradation of the PVE [9] and, as a consequence, alter the characteristics of the PVE, introducing two or more local power peaks rather that one global MPP. This requires modifications of the MPPT algorithm in order to obtain the maximum power out of a serially connected chain of PVEs. It should be noted however, that even though the global MPPT is obtained, the extracted power out of the chain may fall below the maximum power available out of the chain [8].

Several solutions have been proposed and are widely covered in [8]. One of the more energy-efficient solutions is the DPP approach that was widely discussed in chapters 1.6 and 2. This concept applies processing only the power differences between PV elements, thus minimizing conversion losses and improving reliability. The main challenge of present-day DPP-based architectures is the realization of MPPT algorithms on the individual units that are capable of converging to the local MPP of the individual PVE without affecting, or being affected by, the operation of the neighboring PVEs. Solutions to increase the convergence rate toward the MPP while assuring steady-state stability, using modifications of general MPPTs as “perturb and observe” (P&O) and the “hill climbing” (HC) methods implementing variable step size, have been studied in [25], [31] on a centralized unit. Another interesting MPPT concept is the “incremental conductance” (IncCond) [29], [43] in which the algorithm relies on the derivative of the instantaneous power with respect to the voltage, which reduces the mismatch effects and allows more accurate tracking of the MPP.

Most modern MPPT algorithms are realized using digital processing. As a result, issues related to digital control such as sampling resolutions of both current and voltage may introduce undesirable behavior. Power curve traps (PCT) [52] and/or limit cycle oscillations (LCO) [53], [54] may be of major concern for successful MPPT implementation.

The objective of this chapter is to present and explore a new MPPT method that is a hybrid of a modified IncCond method with a dynamic step size operation. The new approach does not require continuous perturbations; it features fast dynamic performance as well as accurate static characteristics for a wide range of insolation levels and is well suited for the use in both centralized or local (i.e. DPP) MPPT. This study further provides a detailed analysis on the effects of digital sampling resolutions that may cause PCT and steady-state LCO.

3.2. *Hybridization of voltage and current power derivatives*

The aim of an MPPT algorithm is to converge into a zero gradient, i.e. $dp_{PV}/dv_{PV} \approx 0$ or $dp_{PV}/di_{PV} \approx 0$. As can be observed from Fig. 3.1, realization of the algorithm based on one of the power derivatives (either current or voltage) results in a proportional but asymmetrical derivative value for regions below and above the MPP [43]. To remedy this, a new derivative factor $e[n]$ that combines two power derivations is defined by:

$$e[n] = \begin{cases} dp_{PV} / dv_{PV} & ; \quad v_{PV} \le V_{MPP} \\ -(dp_{PV} / di_{PV}) & ; \quad v_{PV} > V_{MPP} \end{cases}, \tag{3.1}$$

where v_{PV} and V_{MPP} are the instantaneous and the MPP voltages of the PVE, respectively. By separating the regions below and above V_{MPP}, the derivative factor $e[n]$ has a more symmetrical proportion with respect to the distance from V_{MPP}. It should be noted that merging dp_{PV}/dv_{PV} and dp_{PV}/di_{PV} still results in a smooth function without singularities.

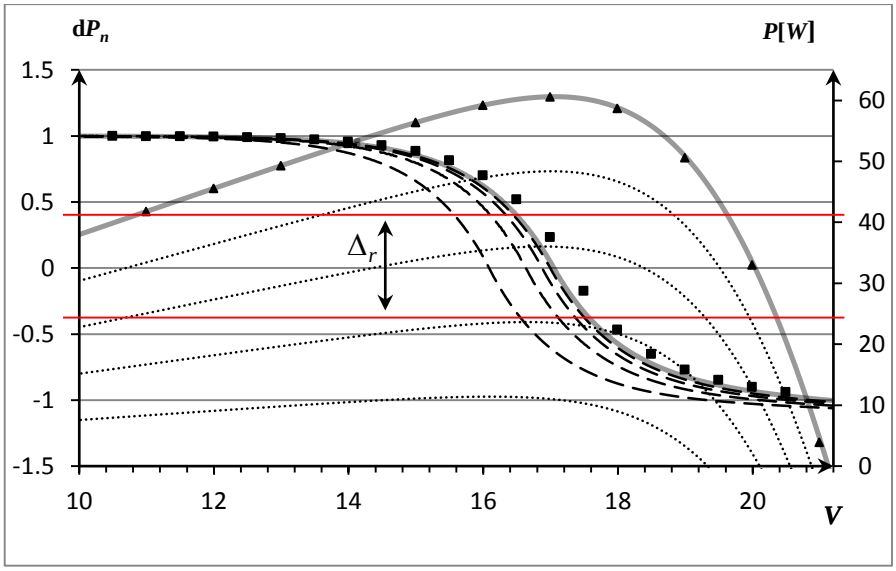

Fig. 3.1 Typical dp_n and power curves as a function of the panel voltage for various insolation levels.

Substituting $p_{PV} = v_{PV} \times i_{PV}$ in (3.1), and after some manipulations, (3.1) can be rewritten as:

$$e[n] = \begin{cases} i_{PV}[n] + \dfrac{\mathrm{d}i_{PV}}{\mathrm{d}v_{PV}} v_{PV}[n] & ; \quad v \le V_{MPP} \\ -\left(v_{PV}[n] + \dfrac{\mathrm{d}v_{PV}}{\mathrm{d}i_{PV}} i_{PV}[n] \right) & ; \quad v > V_{MPP} \end{cases} . \tag{3.2}$$

where the index [n] represents the n^{th} iteration of the algorithm. The differential values of (3.2) can be realized by the controller as:

$$\mathrm{d}p_{PV} = p_{PV}[n] - p_{PV}[n-1] \quad ; \quad \mathrm{d}v_{PV} = v_{PV}[n] - v_{PV}[n-1] \quad ; \quad \mathrm{d}i_{PV} = i_{PV}[n] - i_{PV}[n-1] , \tag{3.3}$$

3.3. *Normalized hybrid incremental conductance (IncCond)*

To expedite the convergence toward the MPP, variable step control is applied based on the value of $e[n]$. A correction signal $A[n]$ (e.g. duty ratio, dead-time, or frequency, depending on the system harvesting converter topology) is generated according to an integral control law, as:

$$A[n] = A[n-1] + K_1 \times K_2[n] \times e[n] , \tag{3.4}$$

where K_1 is the magnitude constant coefficient, and $K_2[n]$ is the integral gain. To facilitate a generic control law for all insolation levels, the integral gain $K_2[n]$ is assigned as a dynamic normalizing factor as:

$$K_2[n] = \begin{cases} \dfrac{1}{i_{PV}[n]} & ; \quad v \le V_{MPP} \\ \dfrac{1}{v_{PV}[n]} & ; \quad v > V_{MPP} \end{cases} . \tag{3.5}$$

Combining (3.2), (3.4) and (3.5) yields a new normalized error signal of the product $K_2 \times e[n]$, named $\mathrm{d}p_n$, which can be expressed as:

$$\mathrm{d}p_n = \begin{cases} 1 + \dfrac{\mathrm{d}i_{PV}}{\mathrm{d}v_{PV}} \times \dfrac{v_{PV}[n]}{i_{PV}[n]} & ; \quad v \le V_{MPP} \\ -\left[1 + \left(\dfrac{\mathrm{d}i_{PV}}{\mathrm{d}v_{PV}} \times \dfrac{v_{PV}[n]}{i_{PV}[n]} \right)^{-1} \right] & ; \quad v > V_{MPP} \end{cases} . \tag{3.6}$$

The resultant $\mathrm{d}p_n$ is bounded within [–1, 1] as depicted in Fig. 3.1. By employing the normalized error, $\mathrm{d}p_n$, the convergence to the MPP is uniform and not affected by the insolation conditions, while preserving a proportional MPP value. To avoid the need of V_{MPP} for selecting

the dp_n expression for the control, the smaller between the two possible dp_n values is selected. A detailed description of the algorithm is given by the flowchart of Fig. 3.2.

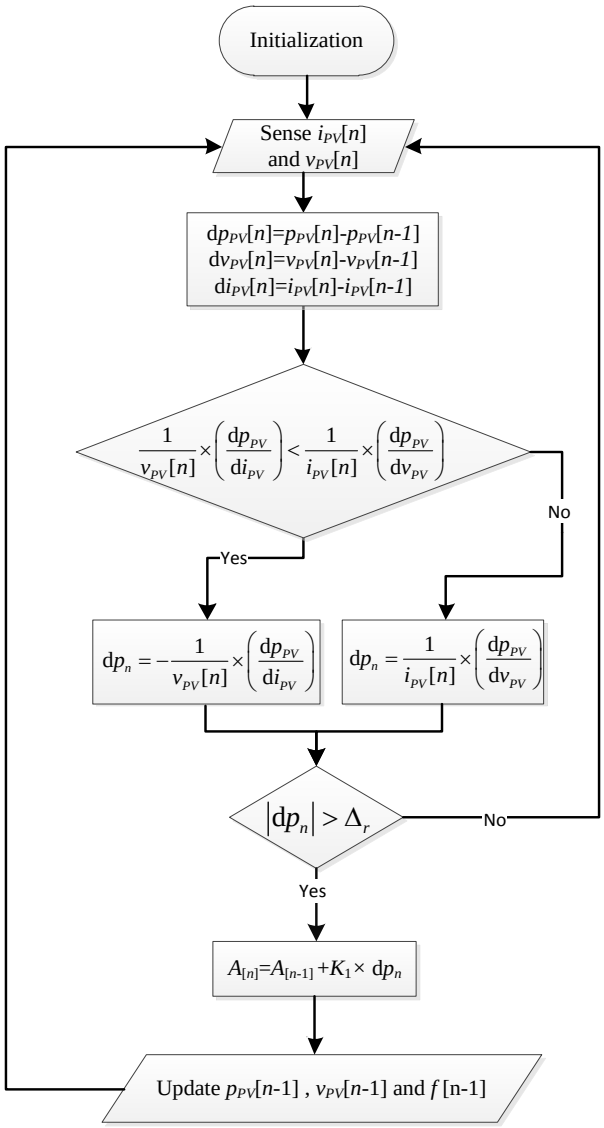

Fig. 3.2 Flowchart of the modified IncCond MPPT algorithm.

The convergence time of the MPPT algorithm and its pattern are primarily dependent on the magnitude constant K_1 that determines the step size of $A[n]$. For small correction steps the convergence would be smooth but slow, whereas large correction steps would result in rapid convergence but may introduce an oscillating error around the MPP. In this work, K_1 has been manually selected to produce the fastest convergence while still maintaining a first-order pattern (i.e., without overshoot).

To employ the above methodology on the proposed GRSCC differential power processing system, the normalized hybrid IncCond MPPT is thus designed to generate a variable step in *f*, proportional to dp_n according to:

$$f[n] = f[n-1] + \Delta f_{max} \mathrm{d}P_n \ , \tag{3.7}$$

where $f[n]$ is the present frequency command generated by the controller governing I_D and the differential current by-passed by the GRSCC between two adjacent PVEs (Fig. 2.1). $f[n–1]$ is the frequency generated in the previous MPPT iteration and Δf_{max} sets the maximum frequency step that is allowed (magnitude constant K_1). The maximum frequency of *f* is bounded by the GRSCC natural frequency, $(3\pi\sqrt{LC})^{-1}$, where no additional delay time is added. The minimum value of *f* is determined by the size of the digital controlled oscillator (DCO) period register.

4. Digital MPPT control phenomena analyses

Convergence of any digital MPPT error signal (dp_n in this particular study) to zero is impractical because of the discrete nature of the control signal $A[n]$ (PWM generated by the DCO). Furthermore, the measured error signal is of a discrete nature as well. The resolution of the measured error signal and the generated control signal $A[n]$ has to be carefully selected to assure stability around MPP, i.e. to avoid limit cycle oscillations [14].

4.1. *Resolution effects on limit cycles*

4.1.1. *Theoretical LCO criterion*

A key criterion for determining the existence of limit-cycle oscillations in a digitally controlled MPPT system relies on the comparison between two main variables. The first is the smallest measurable sensed error signal Δ_r, (i.e., resolution) and the error signal variation due to a LSB change in $A[n]$ [12]–[14], Δ_e. Namely, a necessary condition for no LCO is that Δ_e is smaller than Δ_r. For example, for the proposed MPPT method realized by the system as presented in the block diagram of Fig. 4.1, the criterion for no LCO is:

$$\Delta_e = E_{dpi} \times G_{ia} \times \Delta a_{\mathrm{DCO}} < \Delta_r \quad ; \quad E_{dpi} = \frac{\mathrm{d}(\mathrm{d}p_n)}{\mathrm{d}i_D} \quad ; \quad G_{ia} = \frac{\mathrm{d}i_D}{\mathrm{d}A} \tag{4.1}$$

where Δa_{DCO} is the LSB change of DCO control signal $A[n]$, G_{ia} is the small signal transfer function of the converter (control signal to converter output current value), and E_{dpi} is the small signal transfer function of the PVE in its MPP region (input current to error signal).

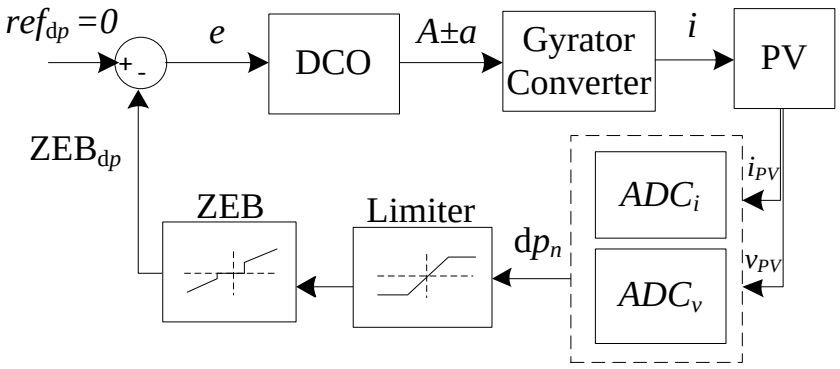

Fig. 4.1 Block diagram of the control system.

Since the error signal is not sensed directly, a practical way to eliminate such oscillations is to decrease the resolution of the calculated error around zero by introducing a zero error bin (ZEB) of size Δ_r. The ZEB is defined such that an absolute value of the calculated error less than Δ_r is considered as zero error, indicating the system has converged to its MPP. The size of Δ_r should be set such that the ZEB contains at least one value of measurable error signal (Fig. 3.1). MPP state unlock condition is designed by sensing dp_{PV} that exceeds a limitation value defined based on the acceptable deviation DC error, Δ_p, from the MPP.

4.1.2. *LCO Analysis for Normalized hybrid IncCond MPPT on GRSCC DPP*

As mentioned previously, convergence of dp_n to zero is impractical because of the discrete nature of f (generated by the digital hardware), and as a consequence dp_n has discrete steps. The condition to avoid LCO (4.1) is redefined individually for the normalized hybrid IncCond MPPT methodology using the GRSCC as a DPP.

The smallest frequency step (1-bit resolution), Δf_{DCO}, that can be generated by the DCO is a function of the time base of the local oscillator, TB, and the running frequency, f_{DCO}. According to [53], Δf_{DCO} can be expressed as:

$$\Delta f_{\mathrm{DCO}} = \frac{1}{N_{\mathrm{per}}\mathrm{TB}} - \frac{1}{\left(N_{\mathrm{per}}-1\right)\mathrm{TB}} \approx \frac{1}{N_{\mathrm{per}}^2\mathrm{TB}} = \mathrm{TB}f_{\mathrm{DCO}}^2, \tag{4.2}$$

where N_{per} is the number of TBs in one period.

Around the MPP, the no-limit-cycles criterion can be expressed as:

$$A_{\mathrm{d}pi} \times G_{if}\left(V_{PV2}\right) \times \Delta f_{\mathrm{DCO}} < \Delta_r \; ; \begin{cases} A_{\mathrm{d}pi} = \dfrac{\mathrm{d}(\mathrm{d}p_n)}{\mathrm{d}i_D} \\ G_{if} = \dfrac{\mathrm{d}i_D}{\mathrm{d}f} \end{cases}, \tag{4.3}$$

where $A_{\mathrm{d}pi}$ is the PV element small-signal gain between the normalized gradient (dp_n) and the differential current (i_D) which can be obtained by taking the derivative of (3.6) with respect to i_D, and $G_{if}\left(V_{PV2}\right)$ is the GRSCC current-to-frequency small-signal gain taking the derivative of (2.3) with respect to f. The block diagram of Fig. 4.4 depicts the control loop of a single GRSCC DPP and the effect of Δf_{DCO} step on dp_n.

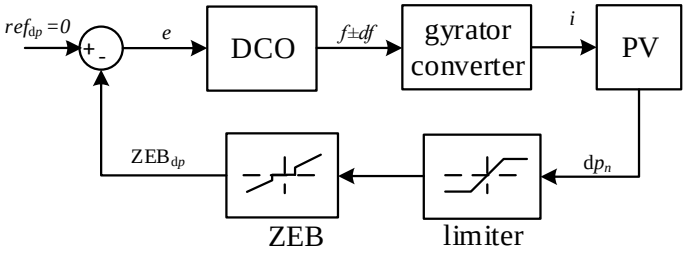

Fig. 4.2 Block diagram of the DPP digital control system.

The derivatives of A_{dpi} and G_{if} around the maximum power point, which is of interest for limit cycles calculation, can be expressed as a function of the system parameters as:

$$A_{dpi}\Big|_{MPP} = \frac{V_{1,MPP}}{I_{1,MPP}}; \quad G_{if}\Big|_{MPP} = 2CV_{2,MPP}\ , \tag{4.4}$$

where $V_{1,MPP}$ and $I_{1,MPP}$ are the controlled PV panel's MPP voltage and current, respectively, $V_{2,MPP}$ is the adjacent PVE MPP voltage, and C is the resonant tank capacitance. It should be noted that the derivative of A_{dpi} has been obtained using a numerical calculation. Having all the relationships of (4.2), and after some manipulations, the no-limit-cycles criterion can be expressed as:

$$\frac{V_{1MPP}}{I_{1MPP}} \times 2CV_{2MPP} \times TBf_{\mathrm{DCO}}{}^{2} < \Delta_r\ . \tag{4.5}$$

The result of (4.5) forms the selection trade-off between the minimum frequency step that is generated and the deviation Δ_r from the true MPP. It implies that in a similar way as in other switch-mode applications, the existence of limit cycle oscillations depends on the command signal generator as well as on the local gain of the converter. However, as opposed to conventional applications where the source has no effect on limit cycles [53], here the characteristics of the PV element also contribute a gain factor to the loop. The tool formed in (4.5), given the system parameters, may assist in the selection of Δ_r and Δf_{max} (noted as K_1 in (4.1)) that will allow rapid convergence to the MPP as well as a tolerable steady-state error.

To demonstrate the behavior of the LCO, a PSIM (Powersim Inc., ver. 9.0) simulation test bench has been constructed and is shown in Fig. 4.2, realizing the normalized hybrid IncCond MPPT algorithm. The algorithm has been applied on a DPP system that comprises a serially connected three-PVE string [1]. The simulated system consists of GRSCC bi-directional

converters connected between every two neighboring PVEs (Fig. 4.2). Every DPP is designed to process the necessary amount of power from the neighboring element.

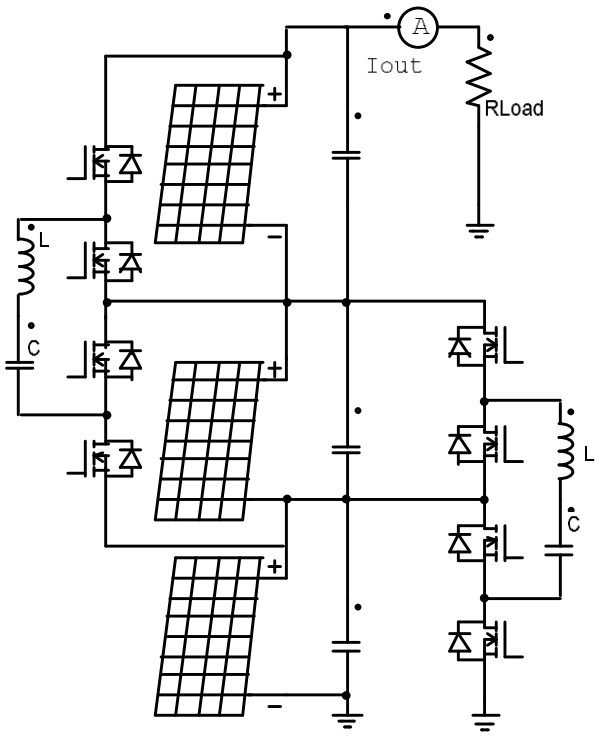

Fig. 4.3 GRSCC-based DPP PV system.

The results in Fig. 4.3a show LCO in the control signal, $A[n]$ (the converter's operating frequency) that generates deviations from the MPP as a result of a too-small Δ_r value. However, in Fig. 4.3b the Δ_r value satisfies (4.5) and yet a DC error can be observed that is due to the relatively large ZEB (i.e. Δ_p) that has been assigned. Fig. 4.3c presents a scenario where all of the PVEs are at their MPP by defining Δ_p=0.4 W.

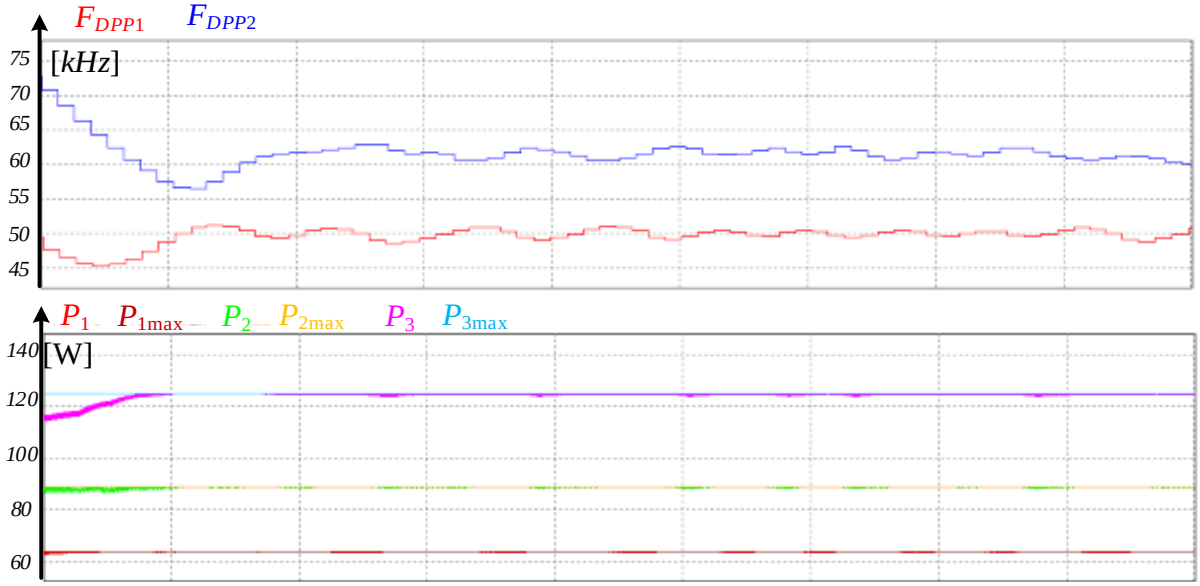
F_{DPP1}
F_{DPP2}
[kHz]
75
70
65
60
55
50
45
P_1
P_{1max}
P_2
P_{2max}
P_3
P_{3max}
[W]
140
120
100
80
60

(a)

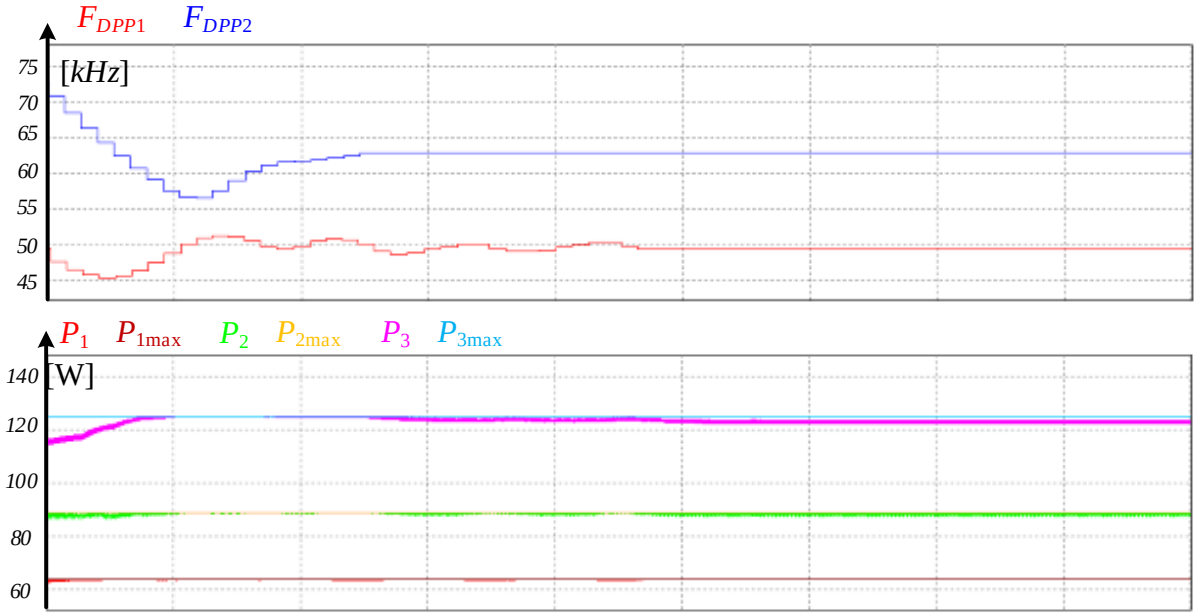
F_{DPP1}
F_{DPP2}
[kHz]
75
70
65
60
55
50
45
P_1
P_{1max}
P_2
P_{2max}
P_3
P_{3max}
[W]
140
120
100
80
60

(b)

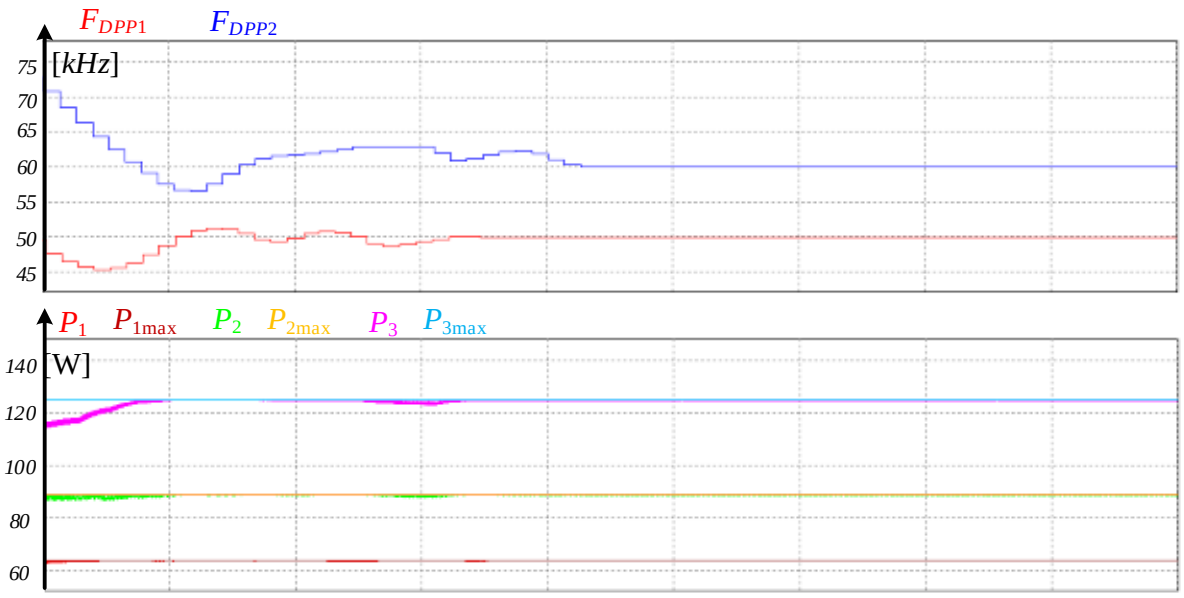

(c)

Fig. 4.4 Simulation results of three PV panels with two DPPs (with $DCO_{Time\text{-}Bais}$=1μsec), demonstrating convergence to the MPP. (a) $\Delta_r = 0.00007$ (b) $\Delta_r = 0.01$ and $\Delta_p = -1$ W (c) $\Delta_r = 0.01$ and $\Delta_p = -0.4$ W.

4.2. *Resolution effects on power curve traps (PCT)*

MPPT algorithms are generally implemented using digital processing; that is, by sampling the required signals (using ADC) and generating a correction action. Poor resolution of the measurement may result in PCT when estimating the power curve or the instantaneous power derivative as can be observed from Fig. 4.5 which illustrates possible measurements scenarios for various resolution settings on the sensed current (i_{PVq}) and voltage (v_{PVq}).

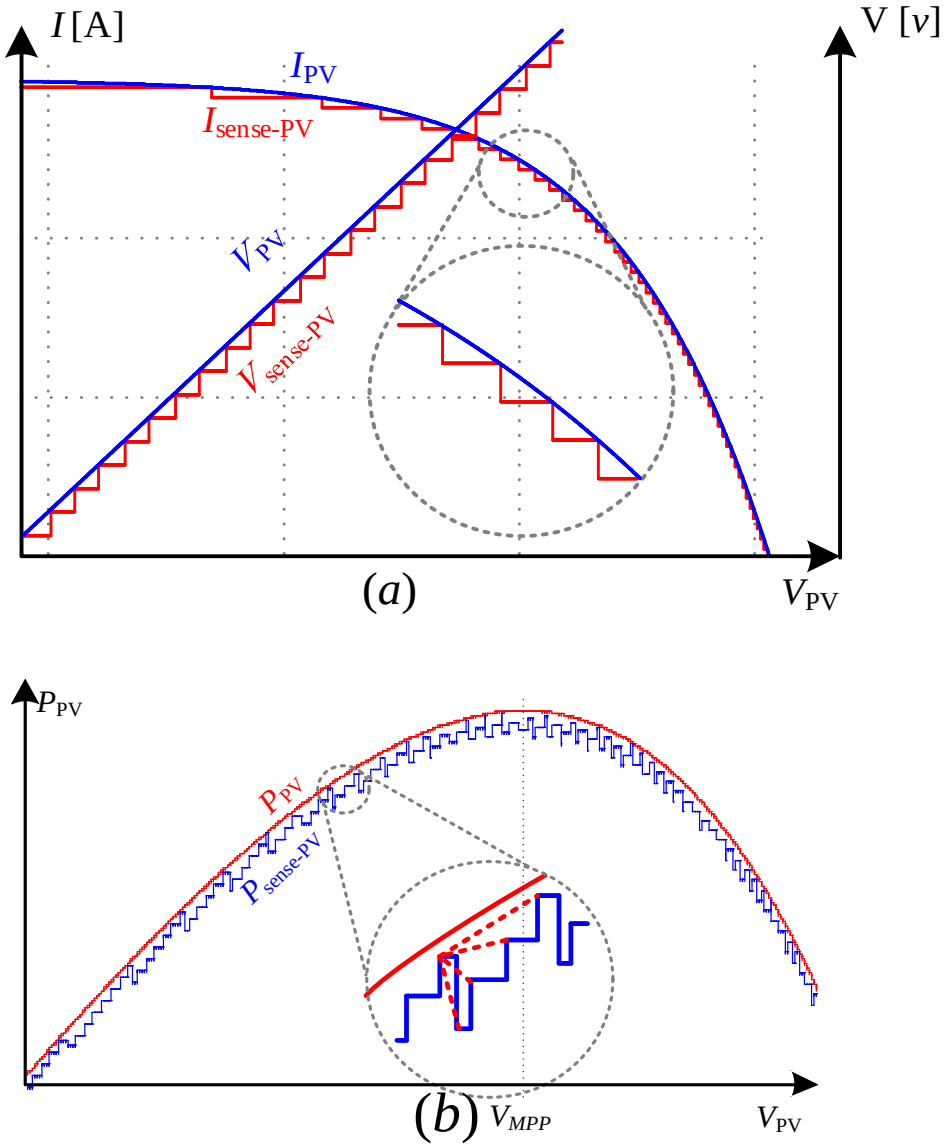

Fig. 4.5 Power traps due to resolution, comparing the true power and the quantized power curves.

Under certain circumstances, PCT may exist in the PVE true power curve, or by the converters modes of operation and other auxiliary effects [52]. This chapter examines those which are created owing to the ADCs' quantization error. The existence of such traps results in erroneous interpretation of the power derivative and causes the algorithm to converge into a false MPP. One possible remedy for this problem can be obtained by averaging the sensed current and voltage, and compensating for any phase lagging due to the moving-average implementation. Another more closed-form solution can be realized by estimating the possible deviation from the true (continuous-form) error signal. This is done by defining the smallest step size of the control signal, $A[n]$, as follows:

The estimation of the possible deviation from the true error signal in the IncCond MPPT method can be calculated by:

$$Err = \left(dp_n\right) - \left(dp_n\right)_q \begin{cases} Err_v & ; \quad v \le V_{MPP} \\ Err_i & ; \quad v > V_{MPP} \end{cases}, \tag{4.6}$$

where $(dp_n)_q$ is the calculated dp_n value (from the PVE-sensed current and voltage), taking into account the quantization effects of the digital platform. The value of *Err* in the vicinity of the PVEs' MPP can be approximated by [29], [43]:

$$\frac{\Delta_i}{\Delta_v} \approx \frac{i_{PV}}{v_{PV}}. \tag{4.7}$$

Therefore, the expression of *Err* is:

$$Err_v = \frac{2q_i}{\Delta_v} \times \frac{v_1}{i_1}\bigg|_{v \approx V_{MPP}} \approx \frac{2q_i}{\Delta_i} \quad ; \quad Err_i = \frac{2q_v}{\Delta_i} \times \frac{i_1}{v_1}\bigg|_{v \approx V_{MPP}} \approx \frac{2q_v}{\Delta_v}, \tag{4.8}$$

where q_i and q_v are the resolution of the current and voltage $ADC_{i/v}$ (potential quantization error). Considering that Err_v and Err_i acquires the greatest value at the MPP and in order to assure power traps avoidance, the $Err_{v/i}$ has to be carefully appointed. The connection between $q_{i/v}$ and the PVE converter step size can be driven from (4.8) by appointing a tolerable $Err_{i/v}$.

However, it can be seen from Fig. 4.5 that most of the power traps are located in the vicinity of the MPP. In the case of locking the operating point on one of them the un-harvested power is negligibly low, but on the other hand locking the operating point on a distant region has a critical effect on the amount of extracted power percentage (related to the potential harvested power).

5. Experimental work

The operation of the differential power architecture has been verified through three independent experiments, the first experiment was carried out on a mini chain of three PV panels to verify the theoretical analysis, the second experiment exemplified the operation on a full-scale grid-connected string and ten panels, and the third experiment was done to compare the operation of a EQSCC to the GRSCC. The GRSCC-based DPP prototypes that were used for the experiments with their specifications are enlisted in TABLE I. The prototype, shown in Fig. 5.1, was realized using an inverting bridge configuration as shown in Fig. 2.1 using PMOS transistors for Q_1 and Q_3 and NMOS for Q_2 and Q_4. The switches were driven by low-side drivers (MIC4427YN), followed by passive DC level-shifters for proper gate driving signals, thoroughly discussed in [4]. Adaptive ZCS and normalized hybrid IncCond MPPT algorithms were implemented digitally on a dsPIC33FJ16GS502. The value of the error window, Δ_r, was selected based on the criterion formed in (4.3), the expression of (4.4), and with some error margin allowing for the tolerance of the practical parameters. The output voltage ripple was measured to be 1.35 V, which is in a very good agreement with the theoretical calculation of (2.6) and (2.8).

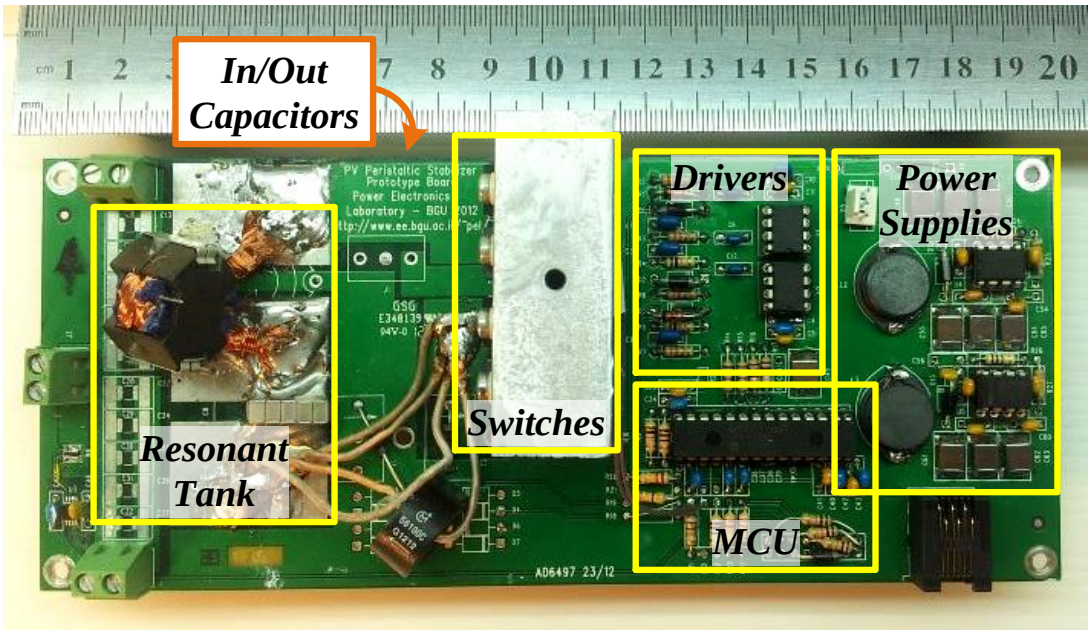

Fig. 5.1 Photograph of the PCB for the DPP GRSCC converter.

TABLE I: PROTOTYPE PARAMETERS FOR THE THREE CONDUCTED EXPERIMENTS

	L	C	C_B	Δ	MOSFETs	P_{max}	f_{max}	η_{max}
Exp. 1	0.5 μH, Ferroxcube RM-8 3F3, A_P=1508×10^{-12} m^4 n=2, ~1mm gap	10×0.1 μF, ceramic	5×10 μF, ceramic	0.14	PMOS: IXTP96P085T NMOS: IXTP160N10T	150 W	130 kHz	91%
Exp. 2,3		5×0.1 μF, ceramic	10×10 μF, ceramic	0.1		120 W	200 kHz	93%

The first experiment was conducted on a string of three 180 W SHARP PV panels (NU-180, E1). The string was connected to a load to manually seek the string MPP. Two DPP prototypes were connected to the string to enable local MPPT. Fig. 5.2 shows the inductor's current and the gating signals for one DPP transferring a differential current of 1.25 A, for a case of an MPP difference of 38% between two adjacent panels. It also shows the added time delay that controls the average current and the effectiveness of the ZCS. Fig. 5.3 demonstrates the convergence of the lower panel towards MPP within a three PV elements string containing two DPPs. The transient was created by switching on its corresponding DPP while the second DPP was connected and running, keeping its panel in MPP. TABLE II summarizes the results of several non-uniform shading conditions and the harvesting factor, ξ (2.2), for each experiment and compares between the operation with and without the DPPs. Fig. 5.4 shows a picture of the testing environment.

TABLE II: HARVEST IMPROVEMENT DUE TO ADDITION OF THE DPPS

$P_{1,MPP}$[a]	$P_{2,MPP}$[a]	$P_{3,MPP}$[a]	P_{max}	ξ_{diodes}[b]	ξ_{DPP}[c]	**Improv.**
0.5	0.95	1	340	0.78	0.94	21%
0.4	0.95	1	327	0.82	0.9	9.3%
0.42	0.74	1	237	0.68	0.96	42%
0.86	1		233	0.94	0.99	5%
0.65	1		200	0.82	0.97	18%
0.54	1		203	0.81	0.95	17%
0.38	1		193	0.68	0.91	33%

a. Normalized to the power of the strongest panel
b. ξ with central inverter only
c. ξ with DPP and a central inverter

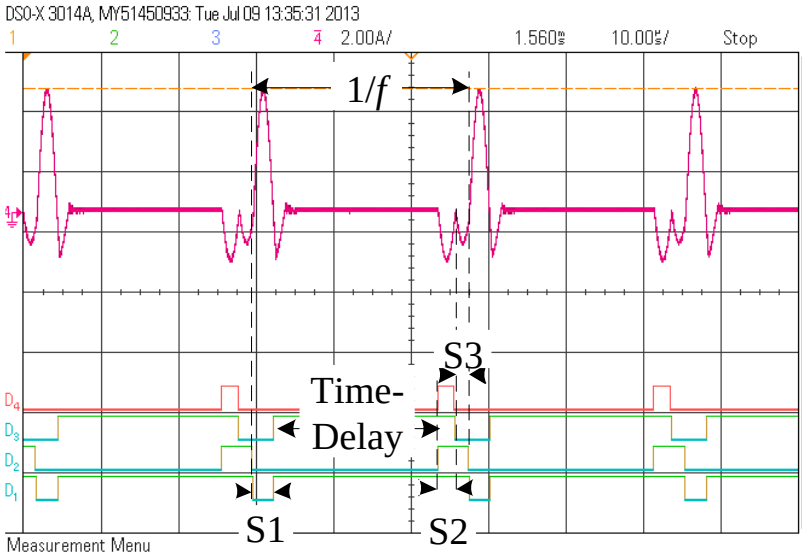

Fig. 5.2 Experimental results of the *L*–*C* tank current and gating signals when processing 1.25 A at *f*=35.8 kHz.

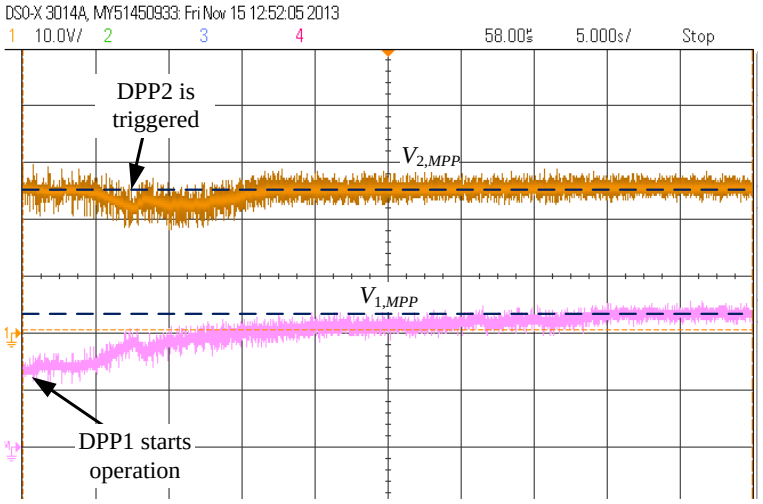

Fig. 5.3 Experimental results showing convergence to the MPP of the entire string of three panels with two DPPs. Top: voltage of PV1 (10 V/div); Bot: voltage of PV2 (10 V/div). Horizontal scale: 5 sec/div.

Fig. 5.4 Photograph of the first outdoor experiment. Beer-sheva, Israel. Friday, Nov. 15, 2013.

The second experiment was conducted on a string of ten 245 W SHARP PV panels (ND-R245A5) connected to an inverter (ND-R245A5) using nine DPP prototypes. Two panels in the string were partially shaded as seen in Fig. 5.5. A second independent string with the same shading conditions, connected to a second inverter was also existent as a control, lacking the DPPs. The test conditions were at an ambient temperature of 16°C and irradiation of approximately 500 W/m^2. TABLE III describes each panel's MPP conditions and the differential power that should be processed to/from the panel.

TABLE III: MPP CONDITIONS AND DIFFERENTIAL POWER DEMANDS FOR THE TESTED STRING

	PV_1	PV_2	PV_3	PV_4	PV_5	PV_6	PV_7	PV_8	PV_9	PV_{10}	**Total**
V_{mpp} **[V]**	26.7	26.7	26.7	26.7	32.3	26.7	30.2	26.7	26.7	26.7	276
I_{mpp} **[A]**	6.27	6.27	6.27	6.27	1.97	6.27	4.11	6.27	6.27	6.27	5.53
P_{mpp} **[W]**	167	167	167	167	64	167	124	167	167	167	1530
P_{diff} **[W]**	-20	-40	-59	-79	36	16	59	40	20		368

The table shows substantial difference both in the MPP voltage and MPP current for panels of different shading levels, demonstrating the demand for a DPP that has step-up/down capabilities. TABLE IV shows the measured results of the two strings (DPP-connected and control) in operation.

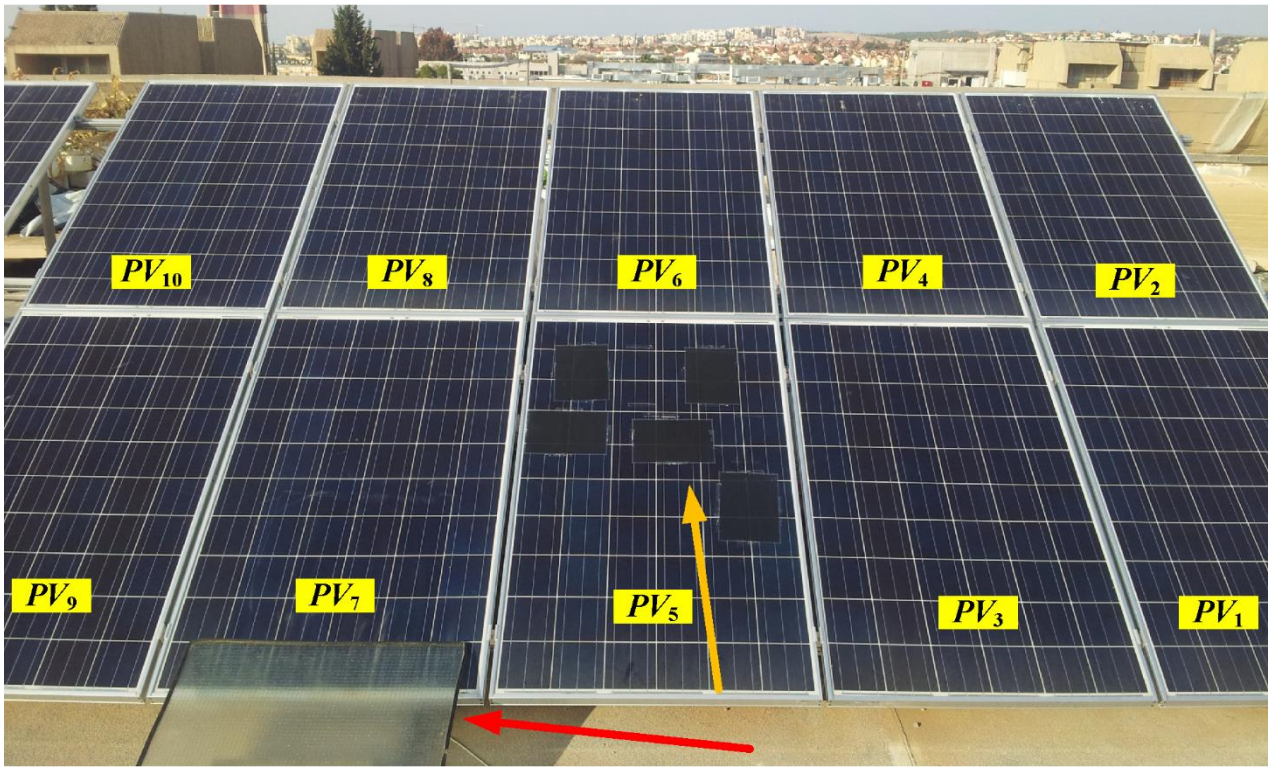

Fig. 5.5 Photograph of the second outdoor experiment. Beer-sheva, Israel. Sunday, Jan. 16, 2014. PV_5 has five A4-sized filters with opacity of 40 %, PV_7 has a diffused glass screen, reducing the irradiation to approximately 75 %.

TABLE IV: RESULTS FOR THE TESTED STRINGS

String	V_{PV1}	V_{PV2}	V_{PV3}	V_{PV4}	V_{PV5}	V_{PV6}	V_{PV7}	V_{PV8}	V_{PV9}	V_{PV10}	V_O	I_O	P_O	ξ
control	32	32	32	32	8.5	32	32	32	32	32	297	3.4	1010	66%
DPPs	27.5	27.5	28	27.5	32	27	24	30	29	28.8	281	4.6	1310	86%

The table shows that using the experimental DPPs aided in extracting an additional 300 W. The power loss due to conversion, estimating a practical efficiency of around 90%, is assumed to be roughly 50 W. This leads to estimated losses of about 170 W due to algorithm mismatch. All the panels can be seen near their MPP voltage with a mismatch of 1 to 2 V, except PV_7. The small mismatch of the panels' voltages is assumed to be from the existence of Δ_r, stopping the MPPT near, but not at, the MPP. The large mismatch of PV_7 can be from a second local MPP located at 24 V caused by the non-uniform shading upon the panel or caused by a power trap that imitates local maximum power points [52]. In the third experiment, conducted on March

12th, 2014, a comparison between DPPs operating as EQSCC, GRSCC, and without DPPs, has been carried out. The PV array was subjected to shading on the same panels as in experiment 2, but with more moderate shading on PV_5 (1 filter sheet instead of 5) to allow comparability to EQSCC operation. TABLE V shows the power that was harvested for the three harvesting methods.

TABLE V: COMPARISON OF THE EXTRACTED POWER USING NO DPP, RSCC, AND GRSCC

String	P_O [W]	ξ
no DPP	1579	79%
RSCC	1789	88%
GRSCC	1809	90%

The GRSCC-based DPP method has been found to be superior to the conventional EQSCC approach even under moderate test conditions and singular differences between the panels. The results further favor the GRSCC method in cases of heavier shadings or if more mismatches exist along the string. In addition, further tuning of the parameter Δ_r and increasing the accuracy of the measurements would result in better convergence toward the MPP; these will be addressed in future publications.

6. Discussion

6.1. *Contributions of the research*

High performance DPP – This work introduces an enhanced DPP topology based on switched-capacitor technology that combines full MPPT capability, high efficiency over wide operation range, and reduced size. The DPP topology based on GRSCC offers a significantly improved technology that leads to a general wide solution for shading or any mismatch problem in PVE power extraction.

Dynamic MPPT algorithm – While most well-known MPPT technics offer long time MPP convergence, the presented dynamic MPPT algorithm obtain MPP by dynamic proportional steps, according to the distance between the present bias working point and the targeted MPP. Furthermore, the proposed MPPT algorithm suits both central and distribute MPPT control.

Limit cycles criterion – A spotlight is placed on the LCO phenomenon and for the first time is analyzed for the convergence problem of MPPT; potential corresponding remedies are proposed.

Power curve traps – The work extends the PCT analysis in PVE research and proposes a few methods to avoid interpreting a power curve trap as MPP.

6.2. *Future work*

GRSCC and EQSCC comparison and combined operation – The different switched capacitor converters discussed in [1] and in [5] use the same hardware design. The different operation is created by the converter's bridge MOSFETs' switching sequence. The converters have different advantages and drawbacks such as efficiency and current or voltage ratio limitations. The EQSCC, for example, can obtain high efficiency during operation with equal voltages because of its input-to-output voltage ratio dependency, yet it cannot provide MPPT control. However, GRSCC compared with EQSCC can gain MPPT control with a better power processing efficiency but its differential current is limited by the converters' highest and lowest operating frequency.

The PV chain length or different types of mismatches between the PVEs' operation points affect the converters' required preferences. A real-time operation analysis of the systems working conditions, evaluating the superior or combined topology (autonomous topology selection GRSCC [1] or EQSCC [5]), will provide a great advantage to the DPP converter.

Sub-module operation – A PV panel generally is composed of tens of serially connected PV cells that generates a similar mismatch phenomenon. Nevertheless, cell-level partial shading is rarer then at the panel level and yet can ruefully injure the PV panel [9]. A cell-level or sub-module version of the DPP converter system can increase the PV harvested power and prevent the PV-degradation which catalyzed by the mismatch conditions.

Integrated-Circuit Integration – The SCC-based DPP architecture presented in this work can be implemented by an IC using the on-chip Si capacitance and stray inductance or using very small additional passive components. An IC design version of the DPP architecture has the ability to adapt to a wide variety of requirements with a generalized simple and effective solution to the partial-shading problem.

7. References

[1] A. Blumenfeld, A. Cervera and M.M. Peretz, "Enhanced Differential Power Processor for PV Systems: Resonant Switched-Capacitor Gyrator Converter with Local MPPT," *IEEE J. Emerging Select. Topics. Power Electron.*, in early access articles 2014.

[2] A. Blumenfeld, A. Cervera and M.M. Peretz, "Enhanced differential power processor for PV systems: Resonant switched-capacitor gyrator converter with local MPPT," in *Proc. 29th Annu. IEEE Appl. Power Electron. Conf. Exposit. (APEC)*, Mar. 2014, pp. 2972–2979.

[3] A. Blumenfeld and M.M. Peretz, "Digital control of PV systems: Dynamic-gain MPPT algorithm and effects of resolution," *in Proc. IEEE 15th Workshop Control Model. Power Electron. (COMPEL)*, 2014, pp. 1–7.

[4] A. Blumenfeld, A. Cervera and S. Ben-Yaakov, "Analysis and design of DC-isolated gate drivers," in *Proc. IEEE 27th Convers. Electr. & Electron. Eng. Israel (IEEEI)*, Nov. 2012, pp. 1–5.

[5] S. Ben-Yaakov, A. Blumenfeld, and A. Cervera, "Design and evaluation of a modular resonant switched capacitors equalizer for PV panels," in *Proc. IEEE Energy Convers. Congr. Exposit. (ECCE)*, Sep. 2012, pp. 4129–4136.

[6] V. V. R. Scarpa, G. Spiazzi, S. Buso, "Low complexity MPPT technique exploiting the effect of the PV cell series resistance," in *Proc. 23rd Annu. IEEE Appl. Power Electron. Conf. Exposit. (APEC)*, Feb. 2008, pp. 1958–19.

[7] T. Esram and P. L.Chapman, "Comparison of photovoltaic array maximum power point tracking techniques," *IEEE Trans. Energy Convers.*, vol. 22, no. 2, pp. 439–449, Jun. 2007.

[8] M. Kasper, D. Bortis, J.W. Kolar, "Classification and Comparative Evaluation of PV Panel-Integrated DC–DC Converter Concepts," *IEEE Trans. Power Electron.*, vol.29, no.5, pp. 2511–2526, May 2014.

[9] K.A. Kim and P.T. Krein, "Hot spotting and second breakdown effects on reverse I–V characteristics for mono-crystalline Si Photovoltaics," in *Proc. IEEE Appl. Power Electron. Conf. Expo. (ECCE)*, Sept. 2013, pp. 1007–1014.

[10] L. L. Buciarelli, B. L. Grossman, E. F. Lyon, and N. E. Rasmussen, "The energy balance associated with the use of a MPPT in a 100 kW peak power system," in *proc. IEEE Photovoltaic Spec. Conf. (PVSC)*, 1980, pp. 523–527.

[11] W. J. A. Teulings, J. C. Marpinard, A. Capel, and D. O'Sullivan, "A new maximum power point tracking system," in *Proc. 24th Annu. IEEE Power Electron. Spec. Conf. (PESC)*, 1993, pp. 833–838.

[12] Y. Kim, H. Jo, and D. Kim, "A new peak power tracker for cost-effective photovoltaic power system," in *Proc. 31st Intersociety Energy Convers. Eng. Conf. (IECEC)*, 1996, pp. 1673–1678.

[13] O. Hashimoto, T. Shimizu, and G. Kimura, "A novel high-performance utility interactive photovoltaic inverter system," *IEEE Trans. on Power Electron.*, vol.18, no.2, pp.704–711, Mar 2003.

[14] E. Koutroulis, K. Kalaitzakis, and N. C. Voulgaris, "Development of a microcontroller-based, photovoltaic maximum power point tracking control system," *IEEE Trans. Power Electron.*, vol. 16, no. 21, pp. 46–54, Jan. 2001.

[15] M.Veerachary, T. Senjyu, andK.Uezato, "Maximum power point tracking control of IDB converter supplied PV system," *in IEE Proc. Elect. Power Applicat.*, 2001, pp. 494–502.

[16] W. Xiao and W. G. Dunford, "A modified adaptive hill climbing MPPT method for photovoltaic power systems," in *Proc. 35th Annu. IEEE Power Electron. Spec. Conf. (PESC)*, 2004, pp. 1957–1963.

[17] O. Wasynczuk, "Dynamic behavior of a class of photovoltaic power systems," *IEEE Trans. Power App. Syst.*, vol. 102, no. 9, pp. 3031–3037, Sep. 1983.

[18] M. A. Slonim and L. M. Rahovich, "Maximum power point regulator for 4kW solar cell array connected through invertor to the AC grid," in *Proc. 31st Intersociety Energy Conver. Eng. Conf. (IECEC)*, 1996, pp. 1669–1672.

[19] C. C. Hua and J. R. Lin, "Fully digital control of distributed photovoltaic power systems," in *Proc. IEEE Int. Symp. Ind. Electron.*, 2001, pp. 1–6.

[20] M. L. Chiang, C. C. Hua, and J. R. Lin, "Direct power control for distributed PV power system," in *Proc. Power Convers. Conf.*, 2002, pp. 311–315.

[21] K. Chomsuwan, P. Prisuwanna, and V. Monyakul, "Photovoltaic grid-connected inverter using two-switch buck-boost converter," in *proc. 29th IEEE Photovoltaic Spec. Conf. (PVSC)*, 2002, pp. 1527–1530.

[22] Y. T. Hsiao and C. H. Chen, "Maximum power tracking for photovoltaic power system," in *Proc. 37th Annu. IAS Meeting Ind. Appl. Conf.*, 2002, pp. 1035–1040.

[23] Y. Jung, G. Yu, J. Choi, and J. Choi, "High-frequency DC link inverter for grid-connected photovoltaic system," *in Proc. 29th IEEE Photovoltaic Spec. Conf. (PVSC)*, 2002, pp. 1410–1413.

[24] S. Jain and V. Agarwal, "A new algorithm for rapid tracking of approximate maximum power point in photovoltaic systems," *IEEE Power Electron. Lett.*, vol. 2, no. 1, pp. 16–19, Mar. 2004.

[25] N. Femia, G. Petrone, G. Spagnuolo, and M. Vitelli, "Optimization of perturb and observe maximum power point tracking method," *IEEE Trans. Power Electron.*, vol. 20, no. 4, pp. 963–973, Jul. 2005.

[26] P. J. Wolfs and L. Tang, "A single cell maximum power point tracking converter without a current sensor for high performance vehicle solar arrays," in *Proc. 36th Annu. IEEE Power Electron. Spec. Conf. (PESC)*, 2005, pp. 165–171.

[27] N. S. D'Souza, L. A. C. Lopes, and X. Liu, "An intelligent maximum power point tracker using peak current control," in *Proc. 36th Annu. IEEE Power Electron. Spec. Conf. (PESC)*, 2005, pp. 172–177.

[28] N. Kasa, T. Iida, and L. Chen, “Flyback inverter controlled by sensorless current MPPT for photovoltaic power system,” *IEEE Trans. Ind. Electron.*, vol. 52, no. 4, pp. 1145–1152, Aug. 2005.

[29] K. H. Hussein, I. Muta, T. Hoshino, and M. Osakada, “Maximum photovoltaic power tracking: an algorithm for rapidly changing atmospheric conditions, ” in *Proc. IEE Generation, Transmission and Distribution*, vol.142, no.1, pp.59,64, Jan 1995.

[30] T. Senjyu and K. Uezato, “Maximum power point tracker using fuzzy control for photovoltaic arrays”, in *Proc. IEEE Int. Conf. lndustrial Technology*, pp. 143–147.

[31] X. Weidong and W.G. Dunford, “A modified adaptive hill climbing MPPT method for photovoltaic power systems,” in *Proc. 35th Annu. IEEE Power Electron. Specialists Conf. (PESC)*, June 2004, pp.1957–1963.

[32] A. F. Boehringer, “Self-adapting dc converter for solar spacecraft power supply,” *IEEE Trans. Aerosp. Electron. Syst.*, vol. AES-4, no. 1, pp. 102–111, Jan. 1968.

[33] E. N. Costogue and S. Lindena, “Comparison of candidate solar array maximum power utilization approaches,” in *Proc. Intersociety Energy Convers. Eng. Conf. (IECEC)*, 1976, pp. 1449–1456.

[34] J. Harada and G. Zhao, “Controlled power-interface between solar cells and ac sources,” in *Proc. IEEE Telecommun. Power Conf.*, 1989, pp. 22.1/1–22.1/7.

[35] A. Brambilla, M. Gambarara, A. Garutti, and F. Ronchi, “New approach to photovoltaic arrays maximum power point tracking,” in *Proc. 30th Annu. IEEE Power Electron. Spec. Conf. (PESC)*, 1999, pp. 632–637.

[36] K. Irisawa, T. Saito, I. Takano, and Y. Sawada, “Maximum power point tracking control of photovoltaic generation system under non-uniform insolation by means of monitoring cells,” in *Proc. 28th IEEE Photovoltaic Spec. Conf. (PVSC)*, 2000, pp. 1707–1710.

[37] T. Y. Kim, H. G. Ahn, S. K. Park, and Y. K. Lee, “A novel maximum power point tracking control for photovoltaic power system under rapidly changing solar radiation,” in *Proc. IEEE Int. Symp. Ind. Electron.*, 2001, pp. 1011–1014.

[38] Y. C. Kuo, T. J. Liang, and J. F. Chen, “Novel maximum-power-point-tracking controller for photovoltaic energy conversion system,” *IEEE Trans. Ind. Electron.*, vol. 48, no. 3, pp. 594–601, Jun. 2001.

[39] G. J. Yu, Y. S. Jung, J. Y. Choi, I. Choy, J. H. Song, and G. S. Kim, “A novel two-mode MPPT control algorithm based on comparative study of existing algorithms,” in *Proc. 29th IEEE Photovoltaic Spec. Conf. (PVSC)*, 2002, pp. 1531–1534.

[40] K. Kobayashi, I. Takano, and Y. Sawada, “A study on a two stagemaximum power point tracking control of a photovoltaic system under partially shaded insolation conditions,” in *Proc. IEEE Power Eng. Soc. Gen. Meet.*, 2003, pp. 2612–2617.

[41] W. Wu, N. Pongratananukul, W. Qiu, K. Rustom, T. Kasparis, and I. Batarseh, “DSP-based multiple peak power tracking for expandable power system,” in *Proc. 18th Annu. IEEE Appl. Power Electron. Conf. Expo. (APEC)*, 2003, pp. 525–530.

[42] K. H. Hussein, I. Muta, T. Hoshino, and M. Osakada, “Maximum photovoltaic power tracking: an algorithm for rapidly changing atmospheric conditions,” in *Proc. IEE Generation, Transmission and Distribution*, vol.142, no.1, pp.59–64, Jan. 1995.

[43] L. Fangrui , D. Shanxu, L. Fei, L.Bangyin, K. Yong, “A Variable Step Size INC MPPT Method for PV Systems,” *IEEE Trans. Ind. Electron.*, vol.55, no.7, pp.2622–2628, Jul. 2008.

[44] K.Kobayashi, I. Takano, and Y. Sawada, “A study on a two stagemaximum power point tracking control of a photovoltaic system under partially shaded insolation conditions,” in *Proc. IEEE Power Eng. Soc. Gen. Meet.*, 2003, pp. 2612–2617.

[45] H. Koizumi and K. Kurokawa, “A novel maximum power point tracking method for PV module integrated converter,” in *Proc. 36th Annu. IEEE Power Electron. Spec. Conf. (PESC)*, 2005, pp. 2081–2086.

[46] M. Sokolov, D. Shmilovitz, “Photovoltaic Maximum Power Point Tracking based on an Adjustable Matched Virtual Load,” in *Proc. 22nd Annu. IEEE Appl. Power Electron. Conf. Expo. (APEC)*, 2007, pp.1480–1484.

[47] E. I. rtiz-Rivera and F. Peng, “A novel method to estimate the maximum power for a photovoltaic inverter system,” in *Proc. 35th Annu. IEEE Power Electron. Spec. Conf. (PESC)*, 2004, pp. 2065–2069.

[48] J. M. Blanes, F. J. Toledo, S. Montero and A. Garrigós, “In-Site Real-Time Photovoltaic I–V Curves and Maximum Power Point Estimator,” *IEEE Trans. Power Electron.*, vol.28, no.3, pp.1234–1240, Mar. 2013.

[49] M. Zhang, J. Wu, and H. Zhao, “The application of slide technology in PV maximum power point tracking system,” in *Proc. 5th World Congr. Intell. Contr. Automat.*, 2004, pp. 5591–5594.

[50] M. Sokolov, D. Shmilovitz, “A Modified MPPT Scheme for Accelerated Convergence,” *IEEE Trans. Energy Conversion*, vol.23, no.4, pp.1105–1107, Dec. 2008

[51] Y. Levron, D. Shmilovitz, “Maximum Power Point Tracking Employing Sliding Mode Control, ” *IEEE Trans. Circuits Syst. I: Regular Papers* , vol.60, no.3, pp.724–732, Mar. 2013.

[52] D.C. Jones and R.W. Erickson, “Probabilistic Analysis of a Generalized Perturb and Observe Algorithm Featuring Robust Operation in the Presence of Power Curve Traps,” *IEEE Trans. Power Electron.*, vol.28, no.6, pp.2912–2926, Jun. 2013.

[53] M.M. Peretz and S. Ben-Yaakov, “Digital control of resonant converters: resolution effects on limit cycles,” *IEEE Trans. Power Electron.*, vol.25, no.6, pp.1652–1661, Jun. 2010.

[54] S. R. Sanders, “On limit cycles and describing function method in periodically switched circuits,” *IEEE Trans. Circuits Syst.*, vol. 40, no. 9, pp. 564–572, Sep. 1993.

[55] Hao Peng, D. Maksimovic, A. Prodic, E. Alarcon, “Modeling of quantization effects in digitally controlled DC–DC converters, ” in *Proc. 35th Ann. IEEE Power Electron. Specialists Conf.(PESC)* 2004, vol.6, pp.4312–4318.

[56] H. Patel, and V. Agarwal, "MATLAB-Based Modeling to Study the Effects of Partial Shading on PV Array Characteristics, " *IEEE Trans. Energy Convers.*, vol. 23, no. 1, pp. 302–310, Mar. 2008.

[57] C. Deline, "Partially shaded operation of a grid-tied PV system," in *Proc. 34th IEEE Photovoltaic Spec. Conf. (PVSC)*, 2009, pp. 1268–1273.

[58] J.J. Cooley and S.B. Leeb, "Per panel photovoltaic energy extraction with multilevel output DC–DC switched capacitor converters," in *Proc. IEEE Appl. Power Electron. Conf. Expo.(APEC)*, 2011, pp. 419–428.

[59] L. Linares, R. W. Erickson, S. MacAlpine, and M. Brandemuehl, "Improved energy capture in series string photovoltaics via smart distributed power electronics," in *Proc. IEEE Appl. Power Electron. Conf. Expo. (APEC)*, Feb. 2009, pp.904–910.

[60] B. Burger, B. Goeldi, S. Rogalla, and H. Schmidt, "Module integrated electronics—An overview," in *Proc. Eur. Photovoltaic Solar Energy Conf. Exhib.*, 2010, pp. 3700–3707.

[61] T. Shimizu, M. Hirakata, T. Kamezawa, and H. Watanabe, "Generation control circuit for photovoltaic modules," *IEEE Trans. Power Electron.*, vol. 16, no. 3, pp. 293–300, May 2001.

[62] Y. Nimni and D. Shmilovitz, "A returned energy architecture for improved photovoltaic systems efficiency," in *Porc. IEEE Int. Symp. Circuits Syst.*, 2010, pp. 2191–2194.

[63] R. Kadri, J. Gaubert, and G. Champenois, "Centralized MPPT with string current diverter for solving the series connection problem in photovoltaic power generation system," in *Porc. IEEE Int. Conf. Clean Elect. Power*, 2011, pp.116–123.

[64] P. S. Shenoy, K. A. Kim, B. B. Johnson, and P. T. Krein, "Differential power processing for increased energy production and reliability of photovoltaic systems," *IEEE Trans. Power Electron.*, vol.28, no.6, pp.2968–2979, Jun. 2013.

[65] M. Kasper, D. Bortis, and J. W. Kolar, "Classification and Comparative Evaluation of PV Panel-Integrated DC–DC Converter Concepts," *IEEE Trans. Power Electron.*, vol.29, no.5, pp.2511–2526, May 2014.

[66] D. Shmilovitz and Y. Levon, "Distributed maximum power point tracking in photovoltaic systems—Emerging architectures and control methods," *Automatika*, vol.53, no.2, pp.142–155, Apr. 2012.

[67] G. R. Walker, J. C. Pierce, "PhotoVoltaic DC–DC Module Integrated Converter for Novel Cascaded and Bypass Grid Connection Topologies — Design and Optimisation, " in *Proc. 37th IEEE Power Electronics Specialists Conference (PESC)*, 2006. pp.1–7.

[68] B. Burger, B. Goeldi, S. Rogalla, and H. Schmidt, "Module integrated electronics—An overview," in *Proc. Eur. Photovoltaic Solar Energy Conf. Exhib.*, 2010, pp.3700–3707.

[69] S.W. Moore and P.J. Schneider, "A review of cell equalization methods for lithium ion and lithium polymer battery systems," in *Porc. SAE World Congr.*, 2001, no. 0959.

[70] K. Sano and H. Fujita, "A resonant switched-capacitor converter for voltage balancing of series-connected capacitors," in *Porc. IEEE Int. Conf. Power Electronics Drive Syst.*, 2009, pp.683–688.

[71] J. T. Stauth, M. D. Seeman, and K. Kesarwani, "Resonant switched-capacitor converters for sub-module distributed photovoltaic power management," *IEEE Trans. Power Electron.*, vol.28, no.3, pp.1189–1198, Mar. 2013.

[72] A. Cervera and M.M. Peretz, "Resonant switched-capacitor voltage regulator with ideal transient response," in *Proc. Appl. Power Electron. Conf. (APEC)*, 2014, pp.867–872.

[73] D. L. King, W. E. Boyson, and J. A. Kratochvil, "Photovoltaic array performance model," *Sandia National Laboratories, Tech. Rep.* SAND2004–3535, 2004.

[74] G. R. Walker, J. Xue, and P. Sernia, "PV string per-module maximum power point enabling converters," in *Proc. Australasian Universities Power Eng. Conf.*, Christchurch, New Zealand, Sep. 28 – Oct. 1, 2003.

[75] C. Olalla, D. Clement, M. Rodriguez, D. Maksimovic, "Architectures and Control of Submodule Integrated DC–DC Converters for Photovoltaic Applications," *IEEE Trans. Power Electron.*, vol.28, no.6, pp.2980–2997, June 2013.

[76] K. Kesarwani, J. T. Stauth, "A comparative theoretical analysis of distributed ladder converters for sub-module PV energy optimization," *in Proc. IEEE 15th Workshop Control Model. Power Electron. (COMPEL)*, 2012, pp.1–6.

[77] S. Ben-Yaakov, "On the Influence of Switch Resistances on Switched Capacitor Converters Losses," *IEEE Trans. Ind. Elect., Letters*, vol. 59, no. 1, pp.638–640, 2012.

[78] S. Ben-Yaakov and M. Evzelman, "Generic and Unified Model of Switched Capacitor Converters," in *Proc. IEEE Energy Convers. Congr. Expo. (ECCE)* 2009, pp.3501–3508.

[79] M. Evzelman and S. Ben-Yaakov, "Average-Current Based Conduction Losses Model of Switched Capacitor Converters", *IEEE Trans. Power Electron.*, vol.28, no.7, pp.3341–3352, 2013.

[80] M. S. Makowski and D. Maksimovic, "Performance Limits of Switched-Capacitor DC–DC Converters", in *Proc. IEEE Power Elect. Specialists Conf. (PESC)* 1995, vol.2, pp.1215–1221.

[81] M. D. Seeman and S. R. Sanders, "Analysis and Optimization of Switched Capacitor DC–DC Converters", *IEEE Trans. Power Electron.*, vol. 23, no. 2, pp.841–851, 2008.

[82] S. Ben-Yaakov and A. Kushnerov, "Algebraic foundation of self adjusting Switched Capacitors Converters," in *Proc. IEEE Energy Convers. Congr. Expo. (ECCE)* 2009 pp.1582–1589.

[83] R. C. N. Pilawa-Podgurski, D. M. Giuliano, and D. J. Perreault, "Merged two-stage power converter architecture with soft charging switched-capacitor energy transfer," in *Proc. IEEE Power Elect. Specialists Conf. (PESC)* 2008, pp. 4008–4015.

[84] S. Lim, J. Ranson, D. M Otten, and D. J. Perreault, "Two-stage power conversion architecture for an LED driver circuit," in *Proc. Appl. Power Electron. Conf. (APEC)* , 2013 pp.854–861.

[85] A. Kushnerov and S. Ben-Yaakov, "Unified algebraic synthesis of generalized Fibonacci Switched Capacitor Converters," in *Proc. IEEE Energy Convers. Congr. Expo. (ECCE)* 2012, pp. 774–778, 2012.

[86] A. Cervera, M. Evzelman, M. Mordechai Peretz, and S. Ben-Yaakov, “A High Efficiency Resonant Switched Capacitor Converter with Continuous Conversion Ratio,” *IEEE Trans. Power Electron.*, in early access articles 2014.

[87] M.M. Peretz and S. Ben-Yaakov, “Digital control of resonant converters: enhancing frequency resolution by dithering,” in *Proc. IEEE Appl. Power Electron. Conf. Expo. (APEC)* 2009, pp.1202–1207.